Mineral Equilibria Constraints on Open-System Melting and Consequences of Melt Loss in Metabasic Rocks

By

Tristan James Stuck, B.Sc (Hons)

Dissertation presented for the degree of Master of Science (M.Sc) in Geology

Department of Geological Sciences

University of Cape Town

Supervisor: Dr J.F.A Diener

December 2016

Abstract

Metabasic rocks constitute a significant proportion of the rock types found within orogenic metamorphic terranes, and the high temperature (T), suprasolidus behaviour of these lithologies provide an important contribution to the process of internal differentiation in the continental crust. The recent development of thermodynamic activity–composition (a–x) relations for high T mineral and melt phases allows the processes of melt generation and segregation to be quantified using high-resolution mineral equilibria modelling for the first time. In this work, calculated Pressure–Temperature (P–T) and Temperature–Mol. % SiO_2 (T–M_{SiO_2}) phase diagrams are used to investigate the suprasolidus evolution of representative amphibolite and eclogite compositions under orogenic P–T conditions in the crust.

Both amphibolite and eclogite compositions are relatively fertile for the production of melt, producing on the order of 30 vol. % by 900 °C and 50 vol. % by 1000 °C during closed-system melting. Melt production in these compositions occurs primarily via the fluid-absent breakdown of hornblende + quartz, under conditions where the fluid pressure (P_f) is less than the total pressure (P_t) - that is ($P_f < P_t$), to produce a pressure-sensitive peritectic assemblage including augite, orthopyroxene and/or garnet, alongside an equilibrium melt.

The introduction of orthopyroxene at the onset of the amphibolite–to–granulite-facies transition at high T results in an increased rate of melt production until either amphibole, or more typically quartz, is exhausted in the rock. Calculated melt compositions are strongly dependent on the starting protolith composition, but initial melting and biotite breakdown produce 1–3 vol. % of K-rich granitic melts. As hornblende melting proceeds, 15–20 vol. % of more sodic tonalite-to-granodioritic melt is produced at higher T, typically until orthopyroxene is introduced and quartz is exhausted.

Further quartz-absent melting results in a rapid change in melt compositions toward more mafic dioritic-to-gabbroic bulk chemistry. Consequently, the SiO_2 content of the protolith exerts a strong first-order control on both the volume and composition of melt produced. High-Si compositions are calculated to be fertile at geologically-realistic P–T conditions, producing considerable granitic melt initially and more subordinate tonalite-granodiorite melt at higher T. By contrast, lower-Si compositions are infertile at these conditions, producing a minor volume of granitic melt, before producing larger volumes of intermediate to mafic melts at ultra-high temperature (UHT) conditions. Ultimately, fertile mafic lithologies are modelled to produce around 20 vol. % granitic melt and 5–10 vol. % more sodic granitoid melt at orogenic P–T conditions, enough to be segregated and make a significant contribution to crustal differentiation.

Whatever proportion of melt is ultimately extracted from the rock, the net effect of melt loss is to inhibit further melt production. The open-system nature of melting in the orogenic crust assists the removal of silica, the alkalis and H_2O from the bulk rock and elevates the melting temperature of the residuum to the P–T conditions of melt extraction. This is such that after 2–3 episodic melt extraction events, the temperatures required to further produce and segregate melt become geologically unrealistic. This will however also depend upon the fraction at which the melt is extracted. These P–T conditions may only be realised in extreme cases of metamorphism and are not applicable to the majority of continental orogenic terranes. Additionally, the removal of melt from the rock greatly increases the preservation potential of two-pyroxene granulite-facies mineral assemblages upon decompression and cooling during exhumation from the P–T_{max} conditions of metamorphism.

Plagiarism Declaration

In submitting this dissertation in electronic and hard copy, I, the undersigned, declare that the work presented in this dissertation is, in its entirety, my own original work, and that any other sources of information used in its compilation have been fully acknowledged. All unreferenced data and/or interpretation contained herein are my own. The work presented in this dissertation has not been submitted, in part or otherwise, to any other tertiary institution or university for any other examination, degree, or qualification and reproduction by the University of Cape Town will not infringe any third party rights.

Tristan J. Stuck

Date: 22/10/2016

Acknowledgements

The author wishes to extend his utmost gratitude and express his appreciation to the research project supervisor, Dr. Johann Diener, for his solid guidance, patience, encouragement and constructive critiques, without which this research project would not have been possible, his time and effort were invaluable.

Further acknowledgement is given to my academic peers and departmental colleagues for many of the interesting discussions and advice throughout the academic year. Finally, many thanks must go to friends and family, for all the support and encouragement to pursue this M.Sc degree and providing never ending motivation.

Contents

Chapter 1

Introduction

Crustal melting and the segregation, upward ascent and concomitant emplacement of granitic magma plays a significant role in the internal chemical differentiation of the modern continental crust (Wells, 1980; Clemens & Vielzeuf, 1987; Vielzeuf *et al.*, 1990; Brown & Solar, 1998a, 1999; Brown, 2001, 2004, 2007a, 2010; Kemp *et al.*, 2007; Sawyer *et al.*, 2011; Brown *et al.*, 2011). High-grade granulite-facies metamorphism in orogenic settings causes the advection of heat and buoyant liquid from lower- to upper-structural levels in the crust.

This will ultimately result in the irreversible differentiation of the precursor continental crust into a rheologically separable evolved felsic upper crust and more residual, dehydrated and mafic lower crust, exhibiting changes to composition and fluid content (e.g. Dewey & Windley, 1981; Clemens, 1990, 2006; Handy *et al.*, 2001; White & Powell, 2002; Jackson *et al.*, 2004; Afonso & Ranalli, 2004; Sawyer *et al.*, 2011).

Evidence for crustal melting and melt segregation is well-documented from leucosome formation in high-grade pelitic migmatites, and investigations of these lithologies has largely shaped our current understanding of the physico-chemical processes associated with open-system melt production and extraction (e.g. Green, 1976; Winkler, 1979; Thompson, 1982; Vielzeuf & Holloway, 1988; Patino-Douce & Johnston, 1991; Harris & Inger, 1992; Sawyer, 1994; Brown *et al.*, 1995, 1999; Brown, 2001, 2002; Milord *et al.*, 2001; Holland & Powell, 2001; White *et al.*, 2001, 2004, 2007; White & Powell, 2002; Korhonen *et al.*, 2010; Yakymchuk & Brown, 2014; Diener & Fagereng, 2014).

Whereas metapelitic compositions are very fertile lithologies, capable of producing significant haplogranite melt volumes, they typically comprise only a relatively minor proportion of exposed high-grade mid- to lower-crustal orogenic settings, and their behaviour is therefore unlikely to be wholly representative of the lower crust. In addition to this, metagreywacke makes up a considerable portion of the crust, often being the dominant siliclastic lithology relative to pelite in regional metamorphic terranes (e.g. Johnson *et al.*, 2008), and from equilibria studies, appear to be significant sources of melt at high T, exceeding 850 °C. Greywacke thus undoubtedly contributes to the chemical differentiation of the crust where it is geologically abundant.

However, multiple sources of evidence suggest that the lower continental crust is characterised chiefly by mafic rock compositions rather than pelite or greywacke, including their geologic occurrence in upper-amphibolite- to granulite-facies terrains (e.g. Harley, 1988), the presence of mafic xenoliths derived from the lower crust in plutonic and volcanic rocks (e.g. Rudnick & Taylor, 1987; Downes, 1993; Condie, 1999), and deep-crustal geophysical inferences (e.g. Christensen & Mooney, 1995; Rudnick & Fountain, 1995; Zandt *et al.*, 1995).

Consequently, the suprasolidus evolution of metamafic rocks and the production of melt from these compositions has been shown to play a significant role for the production of ancient crust during the Archean (e.g. Foley *et al.*, 2002; Martin & Moyen, 2002; Rapp *et al.*, 2003; Moyen & Stevens, 2006; Moyen & Martin, 2012; Johnson *et al.*, 2012, 2014), but may also potentially be expected to play a significant role in the post-Archean evolution of the continental crust (e.g. Drummond & Defant, 1990; Rudnick *et al.*, 1995).

Mineral equilibria modelling techniques have been highly successful in elucidating many aspects of the melting process in metapelites (White *et al.*, 2001; White & Powell, 2002; White *et al.*, 2004, 2007; Korhonen *et al.*, 2010; Yakymchuk & Brown, 2014; Diener & Fagereng, 2014), but this method has not been extensively applied to mafic lithologies because of the absence of appropriate activity–composition (a–x) relations for high-T phases. The recent development of a–x relations for tonalitic melt, high-T amphibole and clinopyroxene (Green *et al.*, 2016) now allows the suprasolidus phase relations in mafic rocks to be quantitatively investigated much more extensively.

In a companion contribution to Green *et al.* (2016), Palin *et al.* (2016) calculated the phase relations, volumes and compositions of melt produced by common, primarily igneous mafic and

intermediate lithologies such as Mid-Ocean Ridge Basalt (MORB), tholeiitic ocean island basalt, calc-alkaline basalt and diorite under orogenic P–T conditions. Their results indicate significant melt production through the high-variance breakdown of hornblende and/or minor biotite, and that intermediate lithologies had greater melt-fertility than basaltic MORB or tholeiite (Palin *et al.*, 2016).

Whereas the results of Palin *et al.* (2016) provide a good first-order description of the melting equilibria for their igneous mafic lithologies, these compositions may not be the most appropriate for investigating the details and consequences of mafic melting in continental orogenic settings in this work, as the precursor basalt may have undergone much more extensive subsolidus change (e.g. Condie, 1989; White & McKenzie, 1989; Arndt & Christensen, 1992; Gallagher & Hawkesworth, 1992; Condie, 1993; Turner & Hawkesworth, 1995; Rudnick *et al.*, 1995) via significant mass-transfer during lower-grade subsolidus metamorphism up to the point at which it first begins to melt, making it's resulting bulk composition inappropriate for describing the melting relations. This has been demonstrated to be true for metapelites (Ague, 1991), and the theory is extended here to the mafic compositions.

This dissertation further develops the novel work of Palin *et al.* (2016) by investigating the high T melting relations in representative metamorphosed mafic lithologies, specifically average bulk-rock compositions of amphibolite and eclogite metabasics. Melting reaction(s) are identified, and P–T conditions and mineral equilibria that control the compositions of melt are investigated. Furthermore the likely volume and absolute composition of melts produced by metamafic lithologies during anatexis under orogenic conditions are estimated.

The project is structured to address the following aims, objectives and questions:

1. Investigate the compositions of metamafic rocks that occur in continental orogenic settings to determine the most appropriate starting bulk rock compositions to use in the phase equilibria modelling calculations. Furthermore, it needs to be be established how appropriate the bulk compositions are for representing the average composition of the lower continental crust.

2. The constraints on open-system melting and batch melt extraction need to be established. Assess the consequences and rheologic implications of melt loss in the lower crust.

3. Determine the phase equilibria constraints on melt production in the crust, and identify

the probable volume and compositions of melt produced by these bulk compositions along geologically-realistic orogenic P–T paths. Particular attention will be given to evaluating: (i) at what T do metamafic rocks begin to melt? (ii) at what T do metamafic rocks produce significant volumes of melt? (iii) what are the the compositions of the melt (iv) what are the first-order controls on melt composition and/or evolution?

4. Identify melting reaction(s) in metamafic rocks, as well as phase(s) that contribute to voluminous melt production. Investigate P–T conditions, and equilibria that produce large volumes of melt and/or increase the rate of melting. Emphasise important phase(s) that control the kinetics of melting in these compositions.

Chapter 2

Literature Review

The following sections cover topics which have been identified as relevant for the overall investigation of the suprasolidus melt evolution in metamafic rocks in this project. The key issues that will be reviewed and examined in this chapter deal with broad areas of: (1) appropriate bulk compositions for modelling; (2) experimental melting of mafic rocks; (3) open-system melting behaviour and percolation thresholds; and (4) recent progress in phase equilibria investigations.

2.1 Low-Grade Metamorphism: Subsolidus Mass Transfer and Chemical Evolution

The rocks found in major orogenic belts display varying degrees of deformation and accompanying metamorphism, and thus the choice of bulk-rock composition to model needs to consider important subsolidus metamorphic processes. These can include volume loss and metasomatic alteration. The study of Ague (1991), although applied to pelites, has demonstrated that subsolidus regional metamorphism is not always an isochemical geological process, and additionally mass transfer and volume strain may account for up to 30 % mass and volume loss up to amphibolite-facies conditions.

Effectively, there is a residual enrichment in low-solubility elements while more soluble elements are removed, fractionating the bulk composition in the process. High-mobility elements include the Large Ion Lithophile (LIL) species Ca, Na and K in pelites.Humphris & Thompson (1978) and Li *et al.* (2000) in their studies of mafic rocks, also show that Na and K are likely remobilised during amphibolite-facies metamorphism. Secondly, the low-grade alteration of the basaltic protolith is well-documented for hydrothermal alteration by seawater (e.g. Mottl & Holland, 1978;

Seyfried & Mottl, 1982) where Si, Ca, Na and K are leached from the basalt at low temperatures (150–300 °C). However, given the relative instability of fluid and absence of excess free fluid in the deep continental crust, this may not be as extensive in continental orogenic rocks, or rocks that are not seafloor basalts (Thompson & Connolly, 1995). Clearly, there are major chemical differences between the bulk compositions of pristine igneous basalt protolith and their metamorphosed equivalents, and any subsolidus chemical change needs to be accounted for in the work presented here.

While the subsolidus chemical history is an important factor, the primary or parental mafic composition that undergoes low-grade chemical change is even more important. Continental collision zones and their associated mobile belts are characterised by metamafic rocks that are not derived from MORB or other oceanic basalt, but rather a chemical variety of continental basalt (e.g. Condie, 1989, 1993, 1999; White & McKenzie, 1989; Arndt & Christensen, 1992; Gallagher & Hawkesworth, 1992; Turner & Hawkesworth, 1995; Rudnick & Fountain, 1995; Rudnick *et al.*, 1995). During continent-continent collision, the predominantly mafic lower crust is pushed to greater depths by lithospheric thickening as a result of compressional tectonism, and the increasing P–T conditions will metamorphose the parental basalt to higher density amphibolite, granulite or eclogite-facies conditions depending on the maximum P and T conditions attained. Burial and heating may induce fluid-absent partial melting and possibly lithospheric delamination contributing to mafic magmatism (Lustrino, 2005). It is these metamafic rocks with continental parental signatures (i.e. calc-alkaline rather than tholeiitic mafic protoliths) that are of interest in modelling continental orogeny, such compositions as found in many Southern African and Antarctic mobile belts (e.g. Jung *et al.*, 2002; Grosch *et al.*, 2007; Diener *et al.*, 2013).

2.2 Experimental Melting of Mafic Rocks: Solidi and H_2O Saturated v. H_2O Undersaturated Melting

Fewer studies (e.g. Holloway & Burnham, 1972; Stern *et al.*, 1975; Helz, 1976) have modelled the water-saturated solidus of the basaltic system. Of these, Stern *et al.* (1975) presents P–T constraints on the fluid-saturated solidus by experimental procedures on three rock compositions representing the calc-alkaline rock series gabbro-tonalite-granite or basalt-andesite-rhyolite, with varying percentages of H_2O, between 600–1300 °C and 1–35 kbar. The fluid-in-excess solidus occurs at 630–650 °C at 10 kbar, with the wet melting curve at slightly higher temperatures at pressures below 10 kbar (∼700 °C at 5 kbar) and the slope of this curve becomes more shallow

at low pressure. The wet melting curve is thus at lower temperature at high P and higher temperature at low P (i.e. negative $\mathrm{d}P/\mathrm{d}T$).

This solidus topology is replicated by Johannes & Holtz (1996), with a similarly shaped wet melting curve for tonalite, but some 30–40 °C higher T, and similar results are noted by Peacock *et al.* (1994) who presents the location of the wet solidus as a combination of data on an olivine tholeiite composition and calculated the H_2O-saturated solidus at ∼650 °C at 1.0 GPa. Thus the temperatures required to *begin* melting an amphibolite under conditions of available excess free crustal fluid apparently compare to, and are even lower, than that required to initiate fluid-present melting of metapelitic compositions (e.g. White *et al.*, 2014).

However, there is much debate in these classical studies on whether metabasalts do actually experience substantial H_2O-saturated melting in the crust, as assumed by Zen *et al.* (1988). In this regard, a number of studies (e.g. Robertson & Wyllie, 1971; Thompson & Connolly, 1995) are of the view that H_2O-absent conditions are more applicable to melting basalt compositions in the lower crust. Expanding on this, they argue that for any considerable melt generation at the P–T of the basaltic wet solidus, a large reservoir of H_2O and similarly large rock porosity is required, and that given the instability of fluid in the earth's crust, any considerable wet melting of basaltic material at temperatures as low as ∼650 °C is unlikely or improbable. They suggest that while H_2O is indeed required to initiate amphibolite melting at appropriate temperatures for crustal orogenesis, residual free water from subsolidus dehydration reactions generates less than 0.5 vol. % melt at the P–T conditions of the fluid-saturated solidus. Furthermore Peacock *et al.* (1994) note that for rock porosities of ∼1 % containing H_2O, the amount of partial melt generated at the wet basaltic solidus is limited to less than 5 vol. %.

Thus fluid-absent melting, which assumes no excess H_2O is available to the melting reaction other than that structurally bound in metamorphic amphibole and/or minor biotite, is an important focus of the majority of the experimental papers concerning the partial melting of basaltic amphibolitic crust. Understanding the position of the fluid-absent solidus of amphibolite is therefore a key prerequisite for investigating the melting relations of metabasic crust within any tectonic setting (Zhang *et al.*, 2013).

One of the earlier studies on metamorphosed basaltic rocks by Beard & Lofgren (1991) investigates the melting relations of five metamorphosed basalts (greenstones and amphibolites) experimentally between 800–1000 °C and 1,3 and 6–9 kbar, focusing on two end-member cases of H_2O availability to the melting system, that of dehydration melting and that of water-saturated melting. In the dehydration melting experiments, the fluid-absent solidus temperature is higher at lower experimental P, with no discernable melt phase at 850 °C at low P. They observe lower solidus temperatures upon increasing the pressure through 6–9 kbar, with petrographically observable melt at 850 °C at higher P. Essentially, the paper describes a fluid-absent solidus with a steep negative slope in P–T space, a positive slope for melt production (i.e. positive $\mathrm{d}M/\mathrm{d}T$) with higher proportions of melt produced at higher P, and increased stability of amphibole to higher P.

Similar experimental constraints on the solidus are presented by Rapp *et al.* (1991) via fluid-absent partial melting of four natural olivine-normative amphibolite rock powders (MORB-like olivine tholeiites, alkali-rich basalts), the major differences being that their solidus is at slightly higher T. The melting curve in their study is seemingly nearly independant of pressure below 20 kbar, at temperatures around ∼950–970 °C. These high suprasolidus T for vapour-deficient melting of amphibolite via hornblende breakdown are bracketed by Peacock *et al.* (1994) at ∼825–1000 °C and 0.5–2.5 GPa, representing continuous amphibole breakdown over nearly 200 °C.

Pioneering studies of major importance to the understanding of dehydration melting of amphibolites are presented by Wyllie & Wolf (1993) and Wolf & Wyllie (1994), who constrain the fluid-absent solidus in P–T space for a simple amphibolite consisting of principally hornblende and plagioclase, and identify two important features; (1) a near-vertical vapour-absent solidus with a steep, positive slope defined by the onset of augite at lower P, and (2) a more subhorizontal curve at higher P where garnet is produced. The conditions for slope change occur at ∼900 °C and 9 kbar and define an 'S-shaped' fluid-absent solidus. This S-shaped solidus has since been reproduced in later studies (e.g. López & Castro, 2001) who constrain it for MORB-derived amphibolite over 4–14 kbar via an incremental heating technique. However, while mimicing the shape, their fluid-absent solidus is some 70–100 °C to lower T at appropriate crustal pressures (below 9–10 kbar). Further reinforcement of similar solidus P–T constraints are given by Zhang *et al.* (2013) for range of synthetic amphibolite compositions, and Vielzeuf & Schmidt (2001).

In summation, it is apparent from the experimental literature that metabasalts may indeed melt at very low T approaching 650–700 °C and to do this requires some free water to be available

to facilitate melting. The presence of (1) minute proportions of H_2O transported to the lower crust in hydrous metamorphic amphibole, and (2) unsegregated low melt fractions retained intergranularly, are essential components which may lower the solidus of the rock to conceivable temperatures relevant to an evolving geotherm (Rapp *et al.*, 1991). However, while they may melt at these low T, the proportion is insignificant and it is accepted that partial melting of metamafic rocks to any meaningful extent such as to contribute to granitoid magmatism is achieved at temperatures well in excess of 800–850 °C at vapour-absent conditions in the crust, and appears to be gradual.

2.3 Experimental Melting of Mafic Rocks: Melting Reactions and the Role of Quartz

Fluid-absent conditions have been demonstrated above to be favoured for the partial melting of metabasalt in the crust. It is therefore important to review how they melt under those conditions. In this regard, Beard & Lofgren (1991) provide two important melt-producing reactions; the first is a lower T reaction which proceeds between 850–900 °C and the second is a higher T reaction which proceeds at substantial temperatures in excess of 900–1000 °C. The initial simplified melt-forming reaction is

$$\text{hornblende} + \text{quartz} + \text{plagioclase} = \text{magnetite} + \text{orthopyroxene} + \text{clinopyroxene} + \text{melt} \quad (2.1)$$

This reaction is terminal to quartz and produces ∼19 vol. % melt by 900 °C. This reaction sees the breakdown of the subsolidus amphibolite assemblage to produce tonalitic melt and a coexisting anhydrous granulite restite assemblage. The unbalanced higher T reaction to produce melt (∼18 vol. %) is given by

$$\text{plagioclase} + \text{clinopyroxene} + \text{orthopyroxene} + \text{ilmenite} + \text{magnetite} = \text{melt} \quad (2.2)$$

Both proposed reactions above importantly represent a continuous multivariate breakdown of hornblende over the range 850–1000 °C and produces voluminous melt (35–40 vol. %). This same reaction describing the incongruent breakdown of amphibole and quartz to produce peritectic orthopyroxene and a large degree of melt is also noted by Rapp *et al.* (1991). While initial solidus melting under conditions of H_2O-saturation has been suggested to occur by the wet melting of plagioclase and quartz, however beyond 850–875 °C plagioclase is not a stable phase and hornblende + quartz ± plagioclase begins to melt to produce the coexisting liquid.

In general the melting reaction at the expense of hornblende, quartz and plagioclase is peritectic with the pressure-dependant formation of either diopsidic-augitic clinopyroxene, enstatitic-pigeonitic orthopyroxene (both low P) and Fe-rich garnet (high P) (López & Castro, 2001).

The importance of quartz in the reacting assemblage on the extent of reaction progress in the dehydration reaction was investigated by Hartel & Pattison (1996). They note that the modal abundance of quartz in the mafic protolith exerted a first-order control on reaction progress, and that whether a given mafic rock was exhausted in either hornblende or quartz first depended on the starting composition of the hornblende + quartz + plagioclase + diopside protolith. In all cases within this study, quartz was depleted first as no hornblende-free residue was noted amongst their granulite samples, and the proportion of quartz therefore controlled the extent of reaction kinetics during melting.

Their mass balance modelling indicates quartz as a reactant with a large coefficient, and that modal hornblende reacts out at thrice the rate of quartz in a given dehydration reaction to produce quartzofeldspathic trondhjemitic melt. Plagioclase too, is given as an important reactant in addition to quartz and hornblende, and defines the dehydration melting of an amphibolite, but it is still quartz-its abundance particularly-that determines reaction extent and not plagioclase. Furthermore, their modelling work reiterates the peritectic formation of garnet and diopside and they note that the most silica-rich protoliths produced the most garnet + diopside rich products, such that more quartz corresponded to more reaction progress.

Additionally, Hartel & Pattison (1996) argue further support for this conclusion is given in the Fe–Mg ratios of the hornblende-garnet-diopside sub-assemblage. The sub-assemblage shows a range of mineral Fe–Mg ratios in different layers of their rocks, and given that all the layers equilibrated under the same P–T conditions, the differing Fe–Mg ratios of the minerals must simply reflect the different P–T conditions at which quartz was consumed in the dehydration melting reaction. Any variation in bulk composition, for example, would rather be manifested in modal proportion differences within the hornblende-garnet-diopside sub-assemblage rather than differing compositional ratios.

2.4 Melt Segregation: Open-System Melting, Physical Percolation Theory and the Melt Percolation Threshold

Once melt has been produced, its segregation and transport mechanism and evolution can be described by two end-member models: (1) batch melting, where a finite proportion of melt (at a given vol. %) is continuously generated in complete liquid-solid equilibrium with the melanosome residue as the P–T conditions of metamorphism progress, and (2) that of fractional melting, which assumes the generated melt is extracted immediately, and only an infinitesimal amount of melt will ever be in equilibrium with the residue at any given time. This results in bulk fractionation once the melt volume in the rock is large enough to form an interconnected permeability network and drain, as per Maaløe & Scheie (1982).

There are two lines of evidence which suggest that open-system behaviour and melt segregation is preferred to operate in the crust: (1) at upper amphibolite- to granulite-facies conditions, metapelites for example, often develop felsic leucosome as a presumed direct indicator of in-situ melt retention. However, it is commonly observed that the composition of the presumed leucosome is not one expected of an equilibrium melt (White *et al.*, 2001); (2) Evidence for prograde metamorphic reactions (e.g. sillimanite + biotite = garnet + cordierite + melt, in pelites) are commonly seen in rocks, but evidence for retrogressive reactions upon cooling are also commonly absent.

In (1) the differing leucosome compositions may represent the peritectic load left behind after melt loss from the leucosome, and additionally the products of fractional crystallization may present significant control on leucosome composition (e.g. Sawyer, 1987). For (2), H_2O is an important component for retrogression, and since it is strongly partitioned into melt when released during dehydration melting, the proportion of H_2O in the rock remains constant unless melt is lost. Thus the low potential for reversal of prograde reactions and apparent lack of retrogressive features may be explained by H_2O-bearing melt loss to the system (White & Powell, 2002, 2010). Either observation can only be explained by open-system geological behaviour, and this has been accepted as the preferred method (Sawyer, 1994; Brown, 2004, 2007b).

If the open-system behaviour of melting is adopted, it raises further question as to the physical process of segregation. Is melt extracted continuously or episodically? In this regard, it is important to consider the rheologic behaviour of melt. At the microscale, the first few percent

melt tend to collect in local dilatant volumes already present when the rock was subsolidus, this is typically at the intersections of grain boundaries in small melt-filled pockets and subsequently pervasive structural fabrics (Sawyer, 2001). Further melt accumulation establishes a localised, pathed network through melt-depleted matrix to feed the development of protoleucosome.

At some point during melt accumulation, enough melt is built up to begin to 'overfill' the diffuse zones and when this point is reached the melt will tend to segregate and displace from the rock, assisted and catalysed greatly by deformation during collisional orogenesis due to the tendency for deformation to be directed towards sites of low strain (i.e. melt-rich protoleucosome), as shown by Vigneresse *et al.* (1996) . The melt is then driven upward in the crust under bouyancy and high melt-wall rock density contrast to regional low-strain areas in the upper crust. The amount of melt required to reach the melt percolation threshold is dependant on a number of factors, including the viscosity, and thereby water content, of the melt (Rushmer, 1991), as well as the characteristics of the source rock, such as grain size and texture. Additional factors include, for example, the strain rate during orogenesis. Thus different thresholds will be valid for different rocks.

A number of contributions have quantified the threshold for predominantly metapelitic rocks, but this has not been applied for mafic/metamafic rocks. Vigneresse *et al.* (1996) investigate the rheologic behaviour of melt in the zone of partial melting and consider physical percolation theory in understanding melting behaviour and the segregation and transfer of melt in the crust. They argue that in-situ retention is improbable and not geologically-realistic, and provide that a minimum of 8 vol. % melt needs to be accumulated in local dilatant sites to overcome their termed Liquid Percolation Threshold (LPT). Above this threshold, intergranular networks assist melt drainage.

Laporte *et al.* (1997) undertook experimental studies on the segregation and permeability thresholds of partially molten crustal protoliths and find that interconnected, grain-scale melt channels may form at very low degrees of melting (< 0.04 vol. %) under static conditions in texturally equilibrated quartzitic rocks and that segregation of melt may operate at these low melt fractions. However, they reason that while segregation potential may be realised, it is relatively inefficient at such low melt volumes due to the high viscosities of the granitic liquids formed. They conclude that an interconnected but stagnant melt network is likely at low degrees of melting, until melt accumulation reaches a few percent, where significant segregation may occur. A connectivity

threshold as low as 3–4 vol. % is suggested for partially molten amphibolite (Laporte & Watson, 1995).

The experimental deformation study of Rosenberg & Handy (2005) is in broad agreement, suggesting that a melt accumulation of 7 vol. % in partially molten granite marks the transition from significant increase in the number melt-bearing grain boundaries to minor increases thereafter, and suggest that a significant strength reduction of the rock occurs between the wet solidus and 7 vol. % melt as a result of the interconnectivity. Overall, the percolation threshold for viscous granite melts in felsic rocks appears, from the amalgamation of experimental studies, to be highly variable but within $\sim$ 5–8 vol. %, depending on the characteristics of the rock.

2.5 Updated a–x Models for Partial Melting of Mafic Rocks and the Mineral Equilibria Approach

.

Experimental contributions to the melting of mafic rocks have until recently provided much of the geological knowledge of suprasolidus behaviour in these compositions. Two recent contributions (Green *et al.*, 2016; Palin *et al.*, 2016) represent the first progress into the high-resolution, quantitative mineral equilibria modelling of mafic rocks at conditions above the H_2O-saturated solidus. The first of these two studies (Green *et al.*, 2016) presents the a–x models, calibrated against experimental thermodynamic data, for tonalitic liquid in mafic systems, allowing for forward modelling in the system Na_2O–CaO–K_2O–FeO–MgO–Al_2O_3–SiO_2–H_2O–TiO_2–Fe_2O_3 (NCKFMASHTO).

Green *et al.* (2016) present two clinopyroxene models: (1) a high-T 'Augite' model which does not include any of the clinopyroxene solvi, but does include Ca-eskolaite and other substitutions that become significant at suprasolidus T conditions, and (2) a low-T 'Omphacite" model, comprising an update of the Green *et al.* (2007) diopside-omphacite-jadeite model for mafic rocks, including the diopside-omphacite and omphacite-jadeite cliopyroxene solvi. Both the high-T augite and tonalitic liquid models are not calibrated for P conditions exceeding 12.5 kbar, and above this pressure the phase equilibria results may not be reliable.

Their high-grade phase equilibria, calculated for a range of mafic compositions including MORB, natural amphibolites and synthetic amphibolites reproduce important experimental melting ob-

servations in the basaltic system, including the construction of an H_2O-saturated solidus with a negative slope (dP/dT), as first determined by pioneering experimental studies concerning basaltic melting relations (e.g. Stern *et al.*, 1975; Wyllie & Wolf, 1993; Wolf & Wyllie, 1994).

The study by Palin *et al.* (2016) uses the tonalitic a–x models to construct a variety of P–T and T–X pseudosections in NCKFMASHTO for compositional variation in mafic rocks, including Mid Ocean Ridge Basalt (MORB) (Sun & McDonough, 1989), tholeiitic basalt (Macdonald, 1968), calc-alkaline basalt (Nockolds & Le Bas, 1977) and Archean Lewisian amphibolite (Park, 1966) protolith compositions in their investigation of high temperature metamorphism. They find that their basaltic compositions are very fertile parent rocks for melt generation and the paper identifies a number of multivariate equilibria contributing to melt production, broadly attributing considerable in-situ melt generation to dehydration melting involving biotite and metamorphic hornblende amphibole and only briefly investigate open-system melting relations.

Their melt compositions correlate to experimental glass compositions produced via hydrate breakdown in natural and synthetic mafic protolith materials (e.g. Beard & Lofgren, 1991; Rushmer, 1991; Wolf & Wyllie, 1994) and appear to be initially granitic in composition, and later melts are calculated to have tonalite-trondhjemite bulk chemistry. Furthermore, they find that intermediate compositions (diorite) are significantly more fertile than MORB, with the diorite producing on the order 50–55 vol. % melt by 900 °C at low-to-intermediate P, in comparison to 25–30 vol. % by MORB. An important conclusion from their modelling is that the onset of the amphibolite-to-granulite transition, defined by prograde stabilisation of orthopyroxene, is extremely sensitive to both bulk-rock oxidation state and bulk H_2O-content.

The recent contributions by Green *et al.* (2016) and Palin *et al.* (2016) are the only recently published literature that utilise the newly-developed melt a–x models to investigate the partial melting of mafic rocks, and they represent only the initial novel progress into the quantitative modelling approach, and there is much need for additional study to build on from this. Particularly with regards to modelling metamorphosed mafic compositions at high T, and this work aims to present further progress in this regard.

Chapter 3

Modelling Considerations

3.1 Phase equilibria calculations and P–T paths

Phase diagrams were calculated using the THERMOCALC software (version 3.45, Powell & Holland, 1988) and an updated version of the Holland & Powell (2011) internally consistent thermodynamic dataset (file tc-ds63.txt, created 05/01/2015). The a–x relations used are: tonalitic melt, high-T augite, hornblende (all from Green *et al.*, 2016), chlorite, biotite, garnet, orthopyroxene, plagioclase–K-feldspar, magnetite–spinel, ilmenite–hematite (all from **?**), and epidote and olivine (Holland & Powell, 2011). Quartz, H_2O, rutile and sphene are pure end-members. Phase abbreviations are as follows: augite (aug), biotite (bi), chlorite (chl), epidote (ep), garnet (g), hematite (hem), hornblende (hb), ilmenite (ilm), K-feldspar (ksp), magnetite (mt), olivine (ol), orthopyroxene (opx), plagioclase (pl), quartz (q), rutile (ru), sphene (sph), melt/liquid (L) and aqueous fluid (H_2O).

Phase proportion modeboxes were constructed using unpublished Mathematica scripts written by Roger Powell (Powell, personal communication). Mineral and melt abundances were output by THERMOCALC as mole fractions, with each phase normalised to one oxide sum total to approximate volume percent. Igneous classification plots, and other geochemical plots relating to the generated melt compositions were constructed using GCDKit v4.1 (Janoušek *et al.*, 2006).

Calculations were performed between 2 and 12 kbar, a range that encompasses the P conditions typical of crustal orogenic metamorphism. Whereas high-P orogenesis can occur at P in excess of 20 kbar, the tonalitic melt model is currently only calibrated for P below 12.5 kbar (Green *et al.*, 2016), and the P–T calculations are constrained accordingly.

A minimum T of 600 °C is chosen for all diagrams as it is below the wet solidus for both rock types and allows sub-and-suprasolidus investigation. High T limits on the calculations are 1050 °C, which may be attainable in certain UHT terranes under unusual circumstances (e.g. Harley, 1988, 1998; Clark *et al.*, 2011) and the equilibria at these extreme temperatures (above 900 °C) are thus of interest. Geologically-realistic orogenic temperatures are on the order of 850–900 °C for the chosen P range (England & Thompson, 1984, 1986; Thompson & England, 1984).

The prograde melt evolution is examined in detail along two isobaric P–T paths at 10 and 5 kbar. These pressure path conditions are a simplification of the prograde history experienced during, collisional orogenesis and low-P 'hot orogeny' metamorphism respectively (e.g. England & Thompson, 1984; Cagnard *et al.*, 2007). Whereas actual P–T vectors will encompass a large range in shape and magnitude, the features described along the chosen idealised paths are considered to be representative and appropriate of suprasolidus processes in metamafic lithologies.

3.2 Bulk rock compositions

The most appropriate compositions for modelling continental orogenic metamorphism consider that the igneous precursor basalt derived from the mantle is calc-alkaline in composition and has undergone a given degree of subsolidus chemical change (e.g. Condie, 1989, 1993, 1999; White & McKenzie, 1989; Arndt & Christensen, 1992; Gallagher & Hawkesworth, 1992; Turner & Hawkesworth, 1995; Rudnick & Fountain, 1995; Rudnick *et al.*, 1995).

We thus consider subsolidus amphibolite and eclogite compositions to be more representative of the lower orogenic continental crust, and more suitable for the modelling purposes in this work. The bulk-rock compositions for equilibria modelling are given in Table 3.2, and are (1) an amphibolite derived from the average of 22 hornblende–plagioclase–quartz ± garnet ± diopside amphibolite samples collected from a number of metamorphic terranes in Southern Africa and Antarctica (see Table 3.1) and (2) an eclogite derived from the average of 16 basaltic eclogites published in the compilation of Jahn *et al.* (2005).

Table 3.1: XRF whole-rock data for 22 amphibolite rock samples from Southern Africa and Antarctica (wt. % oxide).

	NMC, Aggeneys			NMC, Aus					Damara Belt, Namibia				EAO, Malawi				Maud Belt, Antarctica					
	AG-9	Col23	Col28	JDA-087	JDA-003	JDA-028	JDA-033	KMZ-28	MA32V	MA43	GB4	GB5	M-08	M-09	M-16	M-17	SkA 10.1	SkB 11.6	SkA 15.8	S-33	S-53	S-65
SiO_2	47.220	50.910	52.520	49.932	51.420	48.718	49.283	47.489	48.920	43.350	48.030	44.890	43.610	47.039	49.462	48.941	53.750	49.903	48.514	49.307	44.791	45.487
TiO_2	1.677	0.800	0.840	1.714	1.280	3.296	2.091	1.202	1.360	1.510	2.210	1.330	3.013	2.889	2.971	3.715	1.749	2.165	1.038	1.053	1.323	0.909
Al_2O_3	15.173	15.820	15.730	14.913	14.613	12.934	13.444	16.394	14.250	12.600	14.300	9.390	13.869	13.639	12.603	12.200	14.316	14.338	14.993	14.385	14.687	14.454
Fe_2O_3	14.322	10.810	9.920	13.713	12.362	17.151	15.028	11.897	11.280	11.380	12.600	11.560	19.241	18.363	15.725	16.614	14.686	15.304	12.921	11.603	14.214	12.203
MnO	1.048	0.170	0.160	0.214	0.213	0.863	0.264	0.209	0.180	0.190	0.180	0.180	0.283	0.276	0.249	0.222	0.266	0.204	0.298	0.189	0.196	0.165
MgO	6.951	7.190	7.040	6.742	7.229	4.720	6.319	8.539	8.550	6.680	7.080	17.410	6.664	5.854	5.591	5.268	5.446	4.630	8.039	7.186	9.267	12.327
CaO	11.438	11.480	9.260	9.570	10.911	8.646	10.587	9.410	10.940	9.850	9.970	10.030	9.343	8.995	9.175	9.566	7.418	9.407	11.608	9.599	10.126	10.192
Na_2O	0.754	1.150	1.990	0.688	0.521	0.236	0.540	2.097	2.070	2.170	1.360	0.300	1.214	1.321	1.934	1.918	0.464	2.825	0.767	3.067	2.291	1.510
K_2O	0.238	0.220	0.130	1.157	0.782	1.566	0.985	1.241	0.060	0.280	0.810	0.070	1.193	0.972	0.838	0.434	1.008	0.608	0.547	1.661	1.818	0.531
P_2O_5	0.350	0.040	0.090	0.180	0.096	0.300	0.192	0.129	0.070	0.140	0.210	0.130	0.281	0.274	0.299	0.307	0.177	0.240	0.099	0.157	0.096	0.097
SO_3	0.002			0.024	0.034	0.061	0.139	0.003					0.012	0.013	0.004	0.009	0.000	0.006	0.145	0.014	0.020	0.044
Cr_2O_3	0.058			0.030	0.062	0.025	0.047	0.090	0.080	0.040	0.050	0.220	0.013	0.015	0.014	0.012	0.007	0.004	0.018	0.062	0.072	0.121
NiO	0.022			0.006	0.012	0.008	0.010	0.009					0.015	0.014	0.015	0.012	0.017	0.009	0.016	0.033	0.020	0.050
H_2O-	0.024			0.037	0.018	0.027	0.013	0.026	0.059	0.159	0.000	0.000	0.228	0.149	0.210	0.143	0.098	0.096	0.174	0.552	0.073	0.059
LOI	0.481			0.381	0.519	1.077	0.541	1.305	1.359	11.866	1.633	3.779	0.915	0.401	0.659	0.298	0.443	0.032	0.562	0.654	0.578	1.381
Total	99.757	98.590	97.680	99.302	100.073	99.629	99.482	100.039	99.178	100.215	98.433	99.289	99.894	100.213	99.741	99.660	99.843	99.707	99.738	99.521	99.573	99.530

Table 3.2: Bulk compositions (normalised mol. % oxide) used to construct the closed-system P–T pseudosections, modeboxes and T–$M_{\mathrm{SiO_2}}$ section.

	Amphibolite						Eclogite				MORB*
Fig.	4.1a	4.1b	4.1c	7.1a	6.1(M_{Si} = 45; 55)		4.2a	4.2b	4.2c	7.1b	
	P–T	MB^{+}	MB^{+}	P–T	T–$M_{\mathrm{SiO_2}}$		P–T	MB^{+}	MB^{+}	P–T	
SiO_2	49.106	49.337	49.129	46.590	44.995	54.994	48.689	49.121	48.915	46.857	50.086
TiO_2	1.400	1.407	1.401	1.654	1.527	1.249	1.564	1.578	1.572	1.861	1.006
Al_2O_3	8.414	8.453	8.418	8.456	9.178	7.509	9.016	9.096	9.058	9.297	8.691
FeO	10.538	10.588	10.543	12.298	11.495	9.406	10.978	11.076	11.029	12.570	7.784
MgO	11.275	11.328	11.281	13.265	12.299	10.064	8.849	8.928	8.890	10.344	12.145
CaO	10.758	10.808	10.763	12.061	11.734	9.601	11.080	11.178	11.131	12.765	11.671
Na_2O	1.402	1.408	1.497	1.326	1.529	1.251	3.082	3.110	3.097	2.840	2.498
K_2O	0.506	0.508	0.506	0.103	0.552	0.451	0.231	0.233	0.232	0.061	0.215
O	1.217	1.223	1.218	1.438	1.328	1.087	1.373	1.385	1.379	1.633	0.467
H_2O	5.384	4.939	5.340	2.810	5.363	4.388	5.137	4.296	4.696	1.770	5.437

*MORB composition of Sun & McDonough (1989), as per Palin *et al.* (2016).

\+ Modebox diagrams

Bulk compositions were reduced into the 10-component Na_2O–CaO–K_2O–FeO–MgO–Al_2O_3–SiO_2–H_2O–TiO_2–O (NCKFMASHTO) system by ignoring the minor component Cr_2O_3, whereas the exclusion of P_2O_5 was accommodated and corrected for by assuming it is exclusively incorporated into apatite, with the bulk-rock value of CaO adjusted accordingly. Modelled H_2O contents were fixed to allow minimal wet melting at the solidus at 5 and 10 kbar. MnO was not included in the calculations because models that incorporate Mn are available for some minerals (White *et al.*, 2014), but models for high-T Mn-bearing clinopyroxene and amphibole are not yet available. The amount of FeO converted to Fe_2O_3 in the amphibolite was chosen such that $X_{\mathrm{Fe^{3+}}} \sim 0.25$, in agreement with values typical for metamorphosed mafics (e.g. Jahn *et al.*, 2005; Rebay *et al.*, 2010). For the eclogite compositions, measurements for both FeO and Fe_2O_3 were provided in Jahn *et al.* (2005).

The MORB composition, as modelled by Palin *et al.* (2016) is included for comparison in Table 3.2. The amphibolite and eclogite are slightly depleted in SiO_2 and CaO and slightly enriched in TiO_2 and K_2O relative to MORB. The amphibolite is slightly depleted, and the eclogite slightly enriched in Al_2O_3 compared to MORB. Both the amphibolite and eclogite are enriched in FeO and depleted in MgO relative to MORB. The Na_2O content is variable, with the amphibolite being strongly depleted in Na compared to MORB, whereas the eclogite is notably enriched relative to both other lithologies. These differences are likely due to a combination of original chemical differences between continental and oceanic basalts, as well as alteration and mass transfer during lower-grade metamorphism (Humphris & Thompson, 1978; Ague, 1991; Li *et al.*, 2000).

3.3 Closed- and open-system melting

Experimental studies on the basaltic system (e.g. Beard & Lofgren, 1991; Rapp *et al.*, 1991; Rushmer, 1991; Wyllie & Wolf, 1993; Wolf & Wyllie, 1994) as well as recent mineral equilibria contributions (Green *et al.*, 2016; Palin *et al.*, 2016) have demonstrated that melt production in mafic rocks is a continuous process spanning a wide P–T, with the modelling studies finding melt generation to occur primarily through the multi-equilibrium breakdown of hornblende between 750 and 950–1000 °C. Once the melt has formed, the evolution of the melt and residue (cf. Sawyer, 2008) can be considered within either a closed or an open system.

In considering open-system melting in this modelling work, the percolation threshold for viscous granite melts, taken to occur over a range of melt volumes encompassing $\sim$ 5–8 vol. % (Maaløe & Scheie, 1982; Sawyer, 1994, 2001; Vigneresse *et al.*, 1996; Laporte *et al.*, 1997; Rosenberg & Handy, 2005), is extended to be true for the mafic compositions considered here as the low T melts are broadly granitic in composition (see below). Although, the lower viscosity of increasingly mafic melts generated at high T may potentially mean that they have a lower percolation threshold, and we take the melt percolation threshold at these higher T to also be 7 vol. % to maintain consistency with recent contributions on open-system melting behaviour (e.g. Yakymchuk & Brown, 2014; Diener & Fagereng, 2014; Mayne *et al.*, 2016; Palin *et al.*, 2016).

Furthermore, the process of melt loss is assumed here to be episodic, rather than continuous (cf. the 'open' and 'conditionally open' systems of Handy *et al.*, 2001), and drainage is taken to occur whenever the percolation threshold (7 mol. %) is reached - with mol. % approximating vol. %. Additionally, melt loss is taken to be efficient, such that the majority of melt (6 mol. %) is drained before the melt network collapses after each drainage event, with only 1 mol. % melt retained in the collapsed network (Sawyer, 1994, 2001), and the network remaining closed until further sufficient melt can accumulate to reactivate the drainage network (i.e. 7 mol. %).

Chapter 4

Modelling Results

4.1 Closed-system melting relations

4.1.1 Amphibolite

The P–T pseudosection for the average amphibolite composition (Table 3.2) is presented in Fig. 4.1a. Subsolidus fields on the diagram are dominated by assemblages containing hornblende, plagioclase, biotite, sphene and quartz ± ilmenite at low P and the higher pressure minerals; garnet, rutile and epidote are additionally present at high P. The H_2O-saturated solidus was fixed at 5 kbar, and occurs between 675–730 °C over the P range, occuring at the lowest T around 7–7.5 kbar, and has a steep slope that is broadly negative (negative $\mathrm{d}P/\mathrm{d}T$), but varies slightly with P depending on the mineral assemblage. The wet solidus has a negative slope, for example, in the presence of plagioclase, but a slightly positive slope where plagioclase is absent from the stable assemblage at P above 7 kbar (Fig. 4.1a).

The mineral assemblage at the wet solidus at 5 kbar is calculated to consist of 70 vol. % hornblende, 3 vol. % biotite, 10 vol. % plagioclase, 15 vol. % quartz, 2 vol. % sphene and 1 vol. % ilmenite with 1–3 vol. % melt (Fig. 4.1b). The assemblage at 10 kbar is similar in mineral proportions, except for an absence of plagioclase and greater abundance of quartz (23 vol. %; Fig. 4.1c).

Augite occurs almost exclusively at suprasolidus conditions above 750 °C over the P range of the pseudosection in this composition (cf. Palin *et al.*, 2016), and is present at ∼ 20 vol. % throughout the investigated P–T range (Fig. 4.1b,c). Prograde orthopyroxene appears at 770–850 °C in garnet-absent assemblages, and coexists with garnet over a limited range of 8–9 kbar above 850–900 °C and is not stable at higher P (Fig. 4.1a).

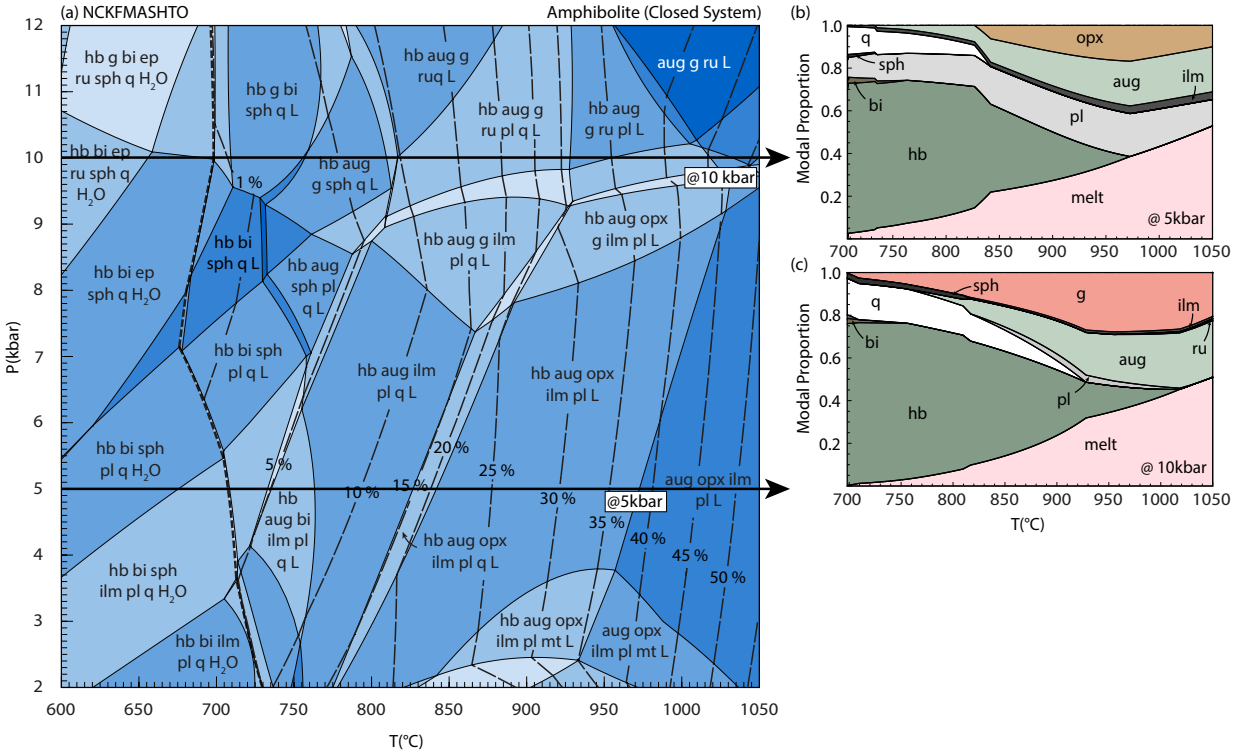

Figure 4.1: (a) P–T pseudosection calculated for the amphibolite bulk composition (Table 3.2) in a closed-system melting environment. The pseudosection is contoured for the modal proportion of melt. (b) and (c): Modeboxes showing the modal abundance of phases at (b) 5 kbar and (c) 10 kbar. Note the 'pulsed' effect of increased melting rate in (a,b) where orthopyroxene is introduced at 5 kbar, and the closely-spaced melt contours superimposed on the orthopyroxene-quartz equilibria in (a)

Orthopyroxene is calculated to constitute up to 15 vol. % of the rock at low P (Fig. 4.1b). Garnet is stable at P between 8–11 kbar over the T range of interest (Fig. 4.1a), and at high T garnet coincides with orthopyroxene. The dual coexistence of orthopyroxene and garnet is P-sensitive. The abundance of hornblende steadily decreases with increasing T as it is consumed through incongruent fluid-absent melting, before being exhausted at 970 °C at 5 kbar and slightly higher T approaching 1020 °C at 10 kbar (Fig. 4.1b,c). There is a notable increase in the rate of hornblende consumption, and melt production, at the conditions where prograde orthopyroxene first appears (e.g. 830–850 °C at 5 kbar; Fig. 4.1b).

The abundance of quartz in the rock also decreases as T increases and melting proceeds, and the assemblages become quartz-absent through consumption of quartz over a 25–30 °C range after orthopyroxene is introduced (Fig. 4.1a). Quartz is consumed more gradually at higher P where the predicted solid peritectic phase is garnet (± augite) instead of orthopyroxene, and consequently persists to higher T in excess of 900 °C in the rock (Fig. 4.1c). Biotite is present in relatively minor proportions (2–3 vol. %) in this composition and it is typically consumed along the prograde path at temperatures approaching 750 °C (Fig. 4.1a).

Calculated melt abundance contours on Fig. 4.1a have a steep, positive slope at lower-P conditions where orthopyroxene is present, but the slope becomes slightly negative in the presence of garnet at higher P (Fig. 4.1a). Melt proportions at the wet solidus are very low at all pressures (1–3 vol. %; Fig. 4.1b,c), and show a steady increase with T such that $\sim$ 30 vol. % is present at 900 °C and more than 50 vol. % is calculated to occur at 1050 °C in a closed-system environment (Fig. 4.1a). The rate of melt production is generally continuous and steady, but there is a notable increase in the melting rate at conditions where orthopyroxene is first introduced, as indicated by the close interval spacing of the melt contours on the P–T pseudosection (Fig. 4.1a) when intersecting the thin orthopyroxene-quartz equilibria. Up to 10 vol. % melt can be rapidly generated over a minute temperature interval until quartz is exhausted in the rock (e.g. 830–850 °C at 5 kbar; Fig. 4.1b).

4.1.2 Eclogite

The P–T pseudosection for the composition of the average eclogite (Table 3.2) in Fig. 4.2a shows a number of topological similarities to that constructed for the amphibolite bulk composition, including subsolidus assemblages that are dominated by hornblende, plagioclase, biotite, sphene and quartz minerals. The H_2O-saturated solidus occurs at 630–715 °C over the P range and has a steep, negative slope with the solidus at lower temperatures at higher P. A higher H_2O content is required in the calculations to stabilise the wet solidus at high P, and consequently the bulk composition is oversaturated in H_2O by 0.5 mol. % at lower P, resulting in the presence of multiple H_2O-bearing fields immediately to higher T above the solidus (Fig. 4.2a). The mineral assemblage at the wet solidus at 5 kbar is calculated to consist of approximately 65 vol. % hornblende, 25 vol. % plagioclase, 3–5 vol. % sphene, 5 vol. % quartz and 1 vol. % augite (Fig. 4.2b).

The solidus assemblage at 10 kbar contains similar phase proportions, but there is a greater modal abundance of both quartz (10 vol. %) and augite (5 vol. %), whereas the plagioclase content at higher P (10–12 vol. %) is lower (Fig. 4.2c). Augite is a stable subsolidus phase in this composition at lower T (600–700 °C), and its abundance generally never exceeds 15–20 vol. % in the rock at both 5 and 10 kbar (Fig. 4.2b,c). Orthopyroxene has restricted stability and is only present below 6.5 kbar on the pseudosection, where it is stable at around 850 °C and destabilises up-temperature to be consumed by ∼980 °C at low P (Fig. 4.2a). Orthopyroxene never coexists with garnet in this composition, and a maximum proportion of 3–5 vol. % orthopyroxene is calculated to ever be present (Fig. 4.2b). Garnet is stable at 8.5–9 kbar at suprasolidus T and its stability is drastically reduced above 900 °C, where garnet-in shifts to higher P (Fig. 4.2a). At 10 kbar, prograde garnet is stable at 820 °C and reaches a maximum proportion of around 12 vol. % at 925–950 °C before decreasing in abundance to higher T (Fig. 4.2c).

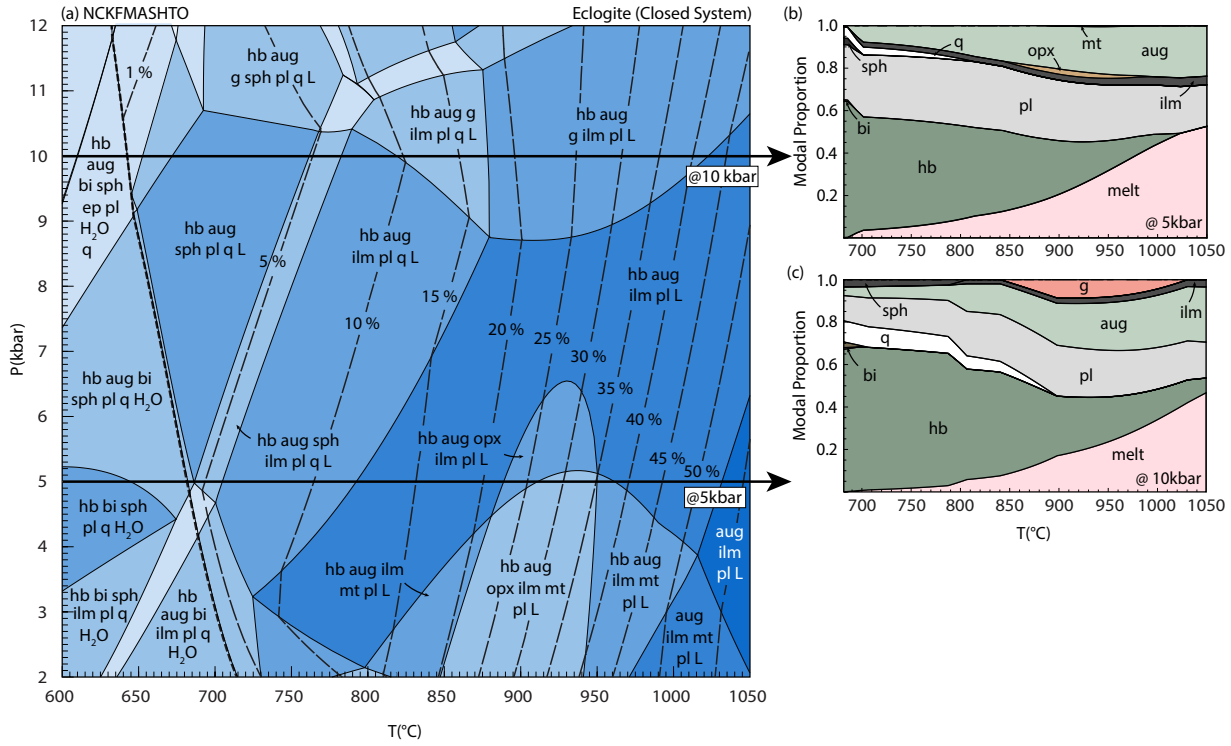

Figure 4.2: (a) P–T pseudosection calculated for the eclogite bulk composition (Table 3.2) in a closed-system melting environment. The pseudosection is contoured for the modal proportion of melt. (b) and (c): Modeboxes showing the modal abundance of phases at (b) 5 kbar and (c) 10 kbar. Note the absence of the 'pulsed' increase in the rate of melting at 5 kbar and that orthopyroxene and quartz never coexist together in the presence of hornblende (b)

Hornblende in the eclogite composition is progressively and steadily consumed by incongruent dehydration melting until it is exhausted at 1025 °C at 5 kbar, whereas at higher P the amphibole persists to beyond 1050 °C at 10 kbar (Fig. 4.2b,c). Unlike the case for the amphibolite, there is no notable increase in the rate of hornblende consumption and/or melt production at low P (Fig. 4.2b). There are however two small but significant increases in the rate of hornblende consumption at 10 kbar along the prograde path, initially at 780–805 °C, corresponding to the exhaustion of sphene in favour of ilmenite and the second at 840–880 °C corresponds to the initial growth of garnet coupled to the depletion of quartz in the rock (Fig. 4.2c). Biotite is a minor phase in the composition and is consumed a few degrees after crossing the wet solidus at P below 9.5 kbar, whereas it may persist to slightly higher temperatures (∼675 °C) at pressures above this.

Calculated melt contours in the eclogite composition have a steep, positive slope in garnet-absent fields at low P, but may have a negative slope at higher P in the presence of both garnet and quartz, as observed for the amphibolite (Fig. 4.2a). The melt contours are evenly spaced and do not show the focused close interval spacing exhibited by the amphibolite at low-to-intermdediate P (Fig. 4.1a). This is likely because orthopyroxene and quartz do not occur in stable equilibrium in this composition at any P–T conditions. Despite this, the overall melt fertility of both the amphibolite and eclogite compositions from solidus temperatures to 1050 °C are comparable, with the eclogite composition producing minor melt at the H_2O-saturated solidus (< 3–5 vol. %), increasing to ∼ 25 vol. % by 900 °C and 50–55 vol. % by 1050 °C (Fig. 4.2a).

4.2 Open-system melting relations

4.2.1 Amphibolite

The pseudosection for the open-system melting of the amphibolite is provided in Fig. 4.3, with the mineral equilibria evolution calculated for successive melt extractions and subsequent bulk-rock fractionations along prograde paths at 5 and 10 kbar (Fig. 4.3a,b). The progressively more fractionated and residual bulk compositions used to construct each of the 'stitched' fragments of the P–T pseudosection are given in Table 4.1. The bulk compositions become progressively more depleted in SiO_2, Na_2O, K_2O and H_2O, and richer in TiO_2, CaO, FeO and MgO as melt extraction proceeds.

Table 4.1: Amphibolite residuum bulk compositions (mol. % oxide) considering episodic melt loss and bulk-fractionation, used to construct the open-system 'stitched' P–T pseudosections in Fig. 4.3a, b.

P	5 kbar								10 kbar					
T(°C)	788	827	843	890	966	1006	1030	1049	803	850	890	922	945	1010
Res.	1st	2nd	3rd	4th	5th	6th	7th	8th	1st	2nd	3rd	4th	5th	6th
SiO_2	48.17	46.929	45.660	44.656	44.165	43.880	43.680	43.515	48.368	47.510	46.590	45.630	44.630	43.876
TiO_2	1.487	1.573	1.663	1.758	1.862	1.976	2.098	2.230	1.481	1.565	1.654	1.748	1.846	1.952
Al_2O_3	8.509	8.574	8.657	8.714	8.737	8.786	8.854	8.929	8.438	8.446	8.456	8.468	8.481	8.449
FeO	11.156	11.716	12.299	12.820	12.949	12.722	12.329	11.880	11.125	11.716	12.298	12.867	13.426	13.805
MgO	11.967	12.627	13.319	14.006	14.518	14.844	15.051	15.169	11.919	12.582	13.265	13.961	14.669	15.292
CaO	11.240	11.669	12.112	12.568	13.052	13.573	14.125	14.704	11.194	11.621	12.061	12.527	13.022	13.513
Na_2O	1.431	1.446	1.447	1.390	1.255	1.116	0.983	0.852	1.406	1.386	1.326	1.219	1.071	0.881
K_2O	0.344	0.215	0.123	0.063	0.032	0.017	0.009	0.000	0.335	0.197	0.103	0.047	0.019	0.007
O	1.293	1.368	1.446	1.529	1.619	1.718	1.825	1.939	1.288	1.361	1.438	1.520	1.605	1.697
H_2O	4.400	3.880	3.270	2.490	1.810	1.370	1.050	0.780	4.45	3.62	2.81	2.01	1.23	0.53

Note that the overall phase diagram topology, mineral assemblages, mineral proportions and solidus equilibria are identical to that of the closed system (Fig. 4.1a) up to the P–T conditions where the initial 7 vol. % melt percolation threshold is reached for the first time. Eight melt loss events are calculated to occur along the 5 kbar path, whereas only six melt loss events occur along the 10 kbar path (Fig. 4.3a,b). The major differences in mineral stability in the open system scenario is that orthopyroxene is introduced at $\sim 30\,^{\circ}$C lower T compared to the closed-system, magnetite stability is increased to higher suprasolidus P–T conditions in excess of 7 kbar, and olivine is present in the strongly fractionated compositions at low P/high T conditions, around $1000\,^{\circ}$C and 5 kbar (Fig. 4.3a,b).

Garnet occurs at slightly lower P ($\sim$1 kbar lower) in the fractionated compositions. The calculated abundance of augite, orthopyroxene and garnet phases are greater in the open-system scenario, with proportions of the clinopyroxene steadily increasing to $\sim$ 15 vol. % by $900\,^{\circ}$C after 4 melt loss events and $\sim$ 35 vol. % by $1050\,^{\circ}$C, after 8 melt loss events at 5 kbar (Fig. 4.3c). The modal abundance of augite increases more rapidly with melt loss at 10 kbar, but the overall proportions are similar to those observed at 5 kbar (Fig. 4.3d). Orthopyroxene and garnet have similar abundances compared to the closed system, with maximum proportions of 15 and 40 vol. % respectively calculated in the rock, but both phases are more stable and abundant to higher T in this open-system scenario (Fig. 4.3c,d).

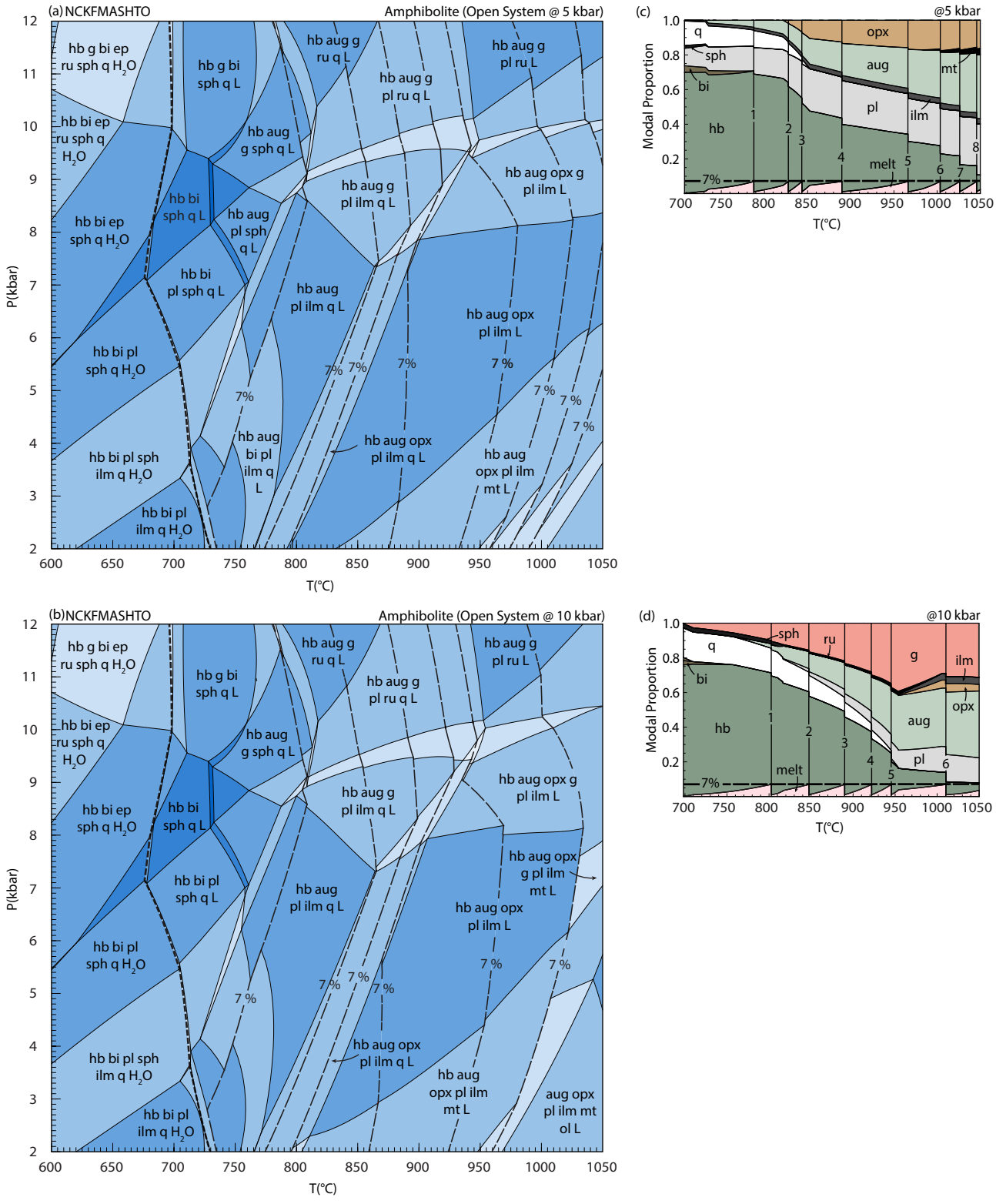

Figure 4.3: P–T pseudosections and modebox diagrams for open-system melting of the amphibolite. (a) Pseudosection considering open-system melting at 5 kbar. (b) Pseudosection calculated for open-system melting at 10 kbar. (c) and (d): Modeboxes showing the modal abundance of phases at (c) 5 kbar and (d) 10 kbar. Bulk compositions used for each 'slice' of the pseudosections are presented in Table 4.1.

Hornblende and quartz are steadily consumed during open-system melting, but hornblende persists a little longer in minor proportions up to 1050 °C at both 5 and 10 kbar (Fig. 4.3c,d). The rate of hornblende consumption is increased in the interval between where orthopyroxene is introduced and quartz is consumed at 5 kbar (825–850 °C; Fig. 4.3c). After this, the rate of hornblende consumption, and melting rate, decreases. A similar trend is observed at 10 kbar, where the rate of hornblende and quartz consumption steadily increases as the terminal stability of quartz is approached at $\sim$ 960 °C (Fig. 4.3d). The rate of hornblende consumption decreases sharply thereafter once quartz is exhausted. The difference for the 8 melt extraction events at 5 kbar and only 6 events at 10 kbar is largely due to continued melt fertility above 950 °C at low P, as both paths have yielded similar melt proportions and five extractions by 960 °C (Fig. 4.3c,d).

4.2.2 Eclogite

The P–T pseudosections for open-system melting of the eclogite composition at 5 and 10 kbar are given in Fig. 4.4a and b respectively, and the bulk compositions used in their construction are provided in Table 4.2. Similar to the amphibolite, eight melt extraction events are modelled to occur along the 5 kbar path, whereas six occur along the 10 kbar path (Fig. 4.4a,b).

Table 4.2: Eclogite residuum bulk compositions (mol. % oxide) considering episodic melt loss and bulk-fractionation, used to construct the open-system 'stitched' P–T pseudosections in Fig. 4.4a,b.

P	5 kbar								10 kbar							
T(°C)	778	859	915	946	969	988	1011	1037	807	866	931	996	1025	1046	1061	1080
Res.	1st	2nd	3rd	4th	5th	6th	7th	8th	1st	2nd	3rd	4th	5th	6th	7th	8th
SiO_2	47.994	47.067	46.436	45.937	45.498	45.079	44.654	44.210	48.167	47.429	46.679	46.170	45.762	45.396	45.046	44.700
TiO_2	1.655	1.751	1.855	1.968	2.090	2.220	2.358	2.505	1.655	1.750	1.852	1.963	2.085	2.215	2.354	2.503
Al_2O_3	9.181	9.302	9.389	9.498	9.629	9.773	9.924	10.078	9.125	9.212	9.277	9.347	9.448	9.568	9.698	9.830
FeO	11.608	12.143	12.342	12.270	12.043	11.753	11.456	11.173	11.591	12.164	12.639	12.622	12.330	11.913	11.443	10.957
MgO	9.360	9.855	10.223	10.461	10.596	10.653	10.652	10.595	9.354	9.862	10.346	10.635	10.793	10.869	10.877	10.823
CaO	11.640	12.196	12.793	13.437	14.124	14.850	15.609	16.400	11.614	12.155	12.718	13.331	13.989	14.684	15.412	16.172
Na_2O	3.071	3.000	2.850	2.682	2.512	2.339	2.156	1.962	3.041	2.965	2.839	2.669	2.508	2.354	2.203	2.053
K_2O	0.143	0.083	0.050	0.031	0.020	0.012	0.008	0.000	0.153	0.097	0.061	0.043	0.031	0.023	0.017	0.012
O	1.452	1.537	1.628	1.727	1.834	1.948	2.069	2.198	1.452	1.536	1.625	1.723	1.829	1.944	2.066	2.196
H_2O	3.900	3.060	2.430	1.990	1.660	1.370	1.110	0.870	3.850	2.830	1.970	1.500	1.220	1.040	0.880	0.760

In comparison to the closed-system scenario, the major difference in mineral stability in the open-system is an increase in the stability of orthopyroxene, and the shift of the amphibolite-to-granulite transition to lower T. Prograde orthopyroxene stabilizes a few degrees after the second melt extraction event at 800–850 °C (Fig. 4.4a,b), and at higher P coexists with garnet at $\sim$ 9

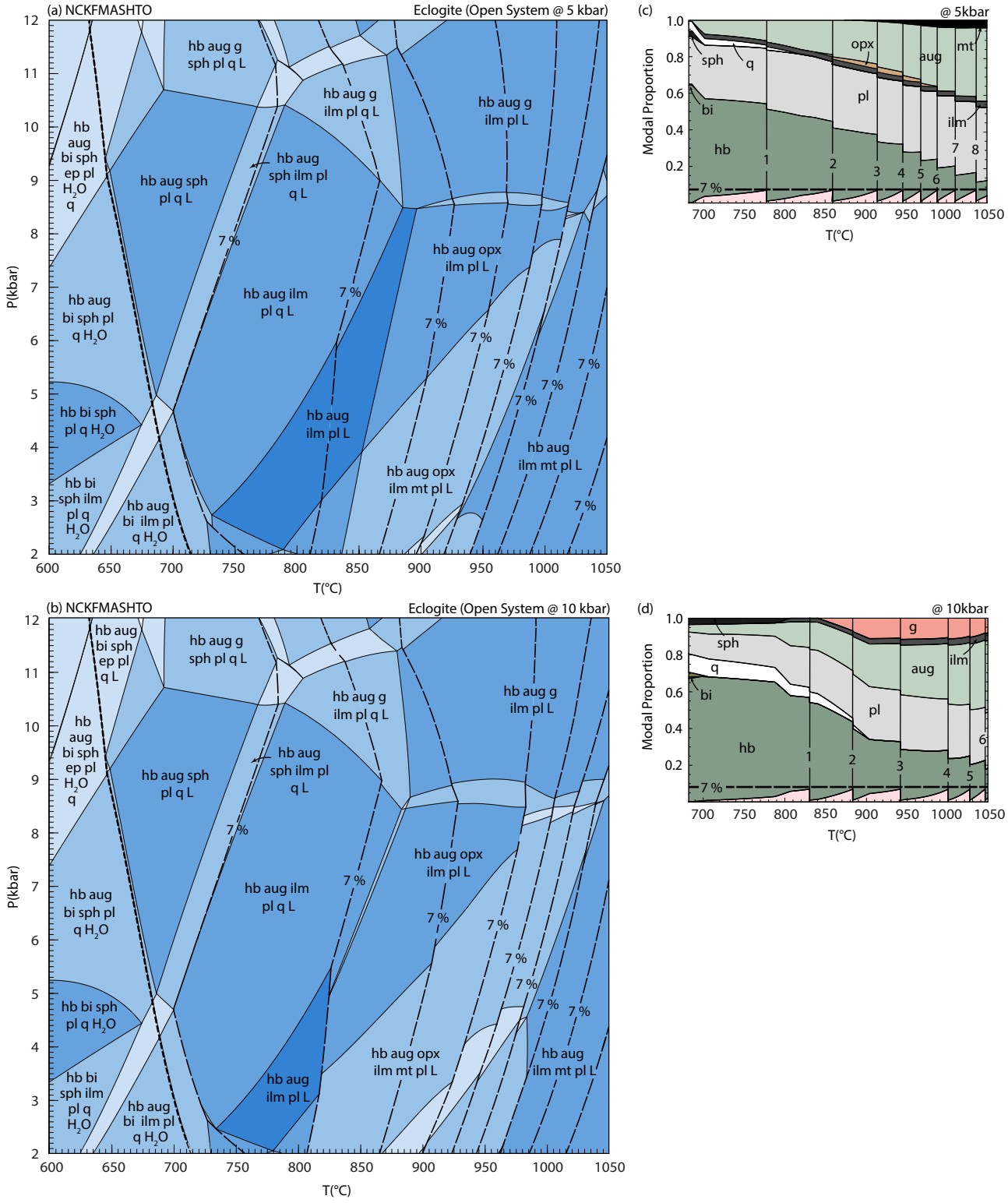

Figure 4.4: P–T pseudosections and modebox diagrams for open-system melting of the eclogite. (a) Pseudosection considering open-system melting at 5 kbar. (b) Pseudosection calculated for open-system melting at 10 kbar. (c) and (d): Modeboxes showing the modal abundance of phases at (c) 5 kbar and (d) 10 kbar. Bulk compositions used for each 'slice' of the pseudosections are presented in Table 4.2.

kbar above 850 °C. Magnetite stability is also increased at low-P/ high-T conditions after melt extraction (Fig. 4.4a,b).

Orthopyroxene is calculated to be present in low modal proportions (2–3 vol. %) in the eclogite composition, whereas augite and garnet abundance are calculated to reach greater proportions of $\sim$ 40 and 10–12 vol. % respectively. Notably, garnet and augite have an expanded suprasolidus P–T stability and are not consumed at high temperature relative to the closed-system scenario (Fig. 4.4c,d). The principal increase in garnet abundance occurs at the expense of hornblende and quartz between 840–900 °C at 10 kbar (Fig. 4.4d).

Hornblende and quartz are both consumed with increasing T and quartz is exhausted at similar T to the closed system case (Fig. 4.4c,d). Hornblende is much more stable in the open system, and at 1050 °C more than 10 vol. % of the amphibole is calculated to still remain in the composition at both 5 and 10 kbar (Fig. 4.4c,d). Whereas the abundance of plagioclase shows a decreasing trend with T in the closed system (Fig. 4.2b,c), the opposite is noted for the open system, where plagioclase abundance appears to increase with T at both 5 and 10 kbar (Fig. 4.4c,d).

At both 5 and 10 kbar, the T interval between melt extraction episodes becomes progressively smaller as the proportion of hornblende in the rock steeply declines by 950–1000 °C (Fig. 4.4c,d). The greater overall melt fertility at 5 kbar, compared to 10 kbar, is due to higher rates of melting at lower T, such that the first extraction event at 5 kbar already occurs at 780 °C, whereas it only occurs at 830 °C at 10 kbar (Fig. 4.4c,d). This may also be a function of the differing H_2O contents at 5 and 10 kbar, with the composition being more hydrated at lower P. There are no marked changes in the rate of melt production related to specific equilibria or P–T conditions for the eclogite within the open-system. This is likely due to orthopyroxene and quartz never being in stable equilibrium.

Chapter 5

Calculated melt compositions

During melting within a closed-system, the melt is retained in-situ in the source region/rock and its initial composition is continuously diluted and homogenised by additional melting and subsequent liquid–solid re-equilibration. However, during open-system melting successive melt batches are segregated and extracted from the source region rather than remaining in-situ, with the composition of each batch determined by the melting reaction(s) at the P–T conditions leading up to the extraction of the given melt batch.

As demonstrated earlier, open-system melting is a more geologically-realistic scenario, and consequently it is chosen to investigate the compositional evolution of successive melt batches extracted from the amphibolite and eclogite compositions during open-system melting. The major element composition of each batch is presented in Table 5.1, and also plotted on the total alkali vs. silica (TAS) diagram (Le Bas *et al.*, 1986), for plutonic rocks after Middlemost (1994), and CaO–Na_2O–K_2O and (FeO+MgO)–K_2O–Na_2O ternary diagrams (Fig. 5.1).

5.1 Amphibolite melt compositions

The initial 5 kbar melts produced from the amphibolite from the solidus (788 °C) to 850 °C (i.e. 1st to 3rd melt fractions) are notably both siliceous (71–73 wt. %) and hydrous (4–5 wt. %) granitic melts (Table 5.1; Fig. 5.1a), which are rich in total alkalis ($>$ 8 wt. %) and especially potassic (4–5.5 wt. %). These initial melts are poorer in Na (1–1.2 wt. %) and the Na:K ratio of the early melts is generally lower ($\sim$ 0.2–0.3). Additionally these low T melts are a reservoir for only very low proportions of FeO and MgO ($<$ 1 wt. %), while being relatively aluminous (12–13 wt %).

At high P (10 kbar) the initial melts from the solidus to 950 °C (i.e. 1st to 5th melt fractions) are silica-rich granitic melts, but relative to the lower P melts they are less siliceous (67–68 wt. %), more aluminous (14–15 wt. %) and more hydrous (6–7 wt. %) batch melts (Table 5.1; Fig. 5.1a). As melting proceeds at both 5 and 10 kbar, the Na:K ratio of the initial melt fractions ($\sim$ 0.25) increases with T as they become more sodic and less potassic at higher fractions.

Table 5.1: Melt batch compositions calculated for open-system melting at 5 and 10 kbar for the amphibolite and eclogite bulk compositions (normalised* wt. % oxide)

P	Amphibolite melts - 5 kbar								Amphibolite melts - 10 kbar						
T(°C)	788	827	843	890	966	1006	1030	1049	803	850	890	922	945	1010	1062
Melt	1st	2nd	3rd	4th	5th	6th	7th	8th	1st	2nd	3rd	4th	5th	6th	7th
SiO_2	71.764	71.850	72.143	67.145	54.911	49.137	46.824	45.903	67.268	67.576	67.587	67.223	66.734	59.705	51.514
Al_2O_3	13.097	12.906	12.616	13.818	14.638	13.546	12.981	12.863	14.753	14.978	14.892	14.797	14.742	15.833	14.496
FeO	0.874	1.744	1.930	3.961	13.273	20.056	22.648	23.110	0.485	0.961	1.850	2.852	3.724	8.370	17.151
MgO	0.162	0.330	0.389	0.929	3.712	6.185	7.686	8.750	0.091	0.193	0.406	0.692	0.996	2.594	5.972
CaO	3.182	3.622	3.843	4.107	4.227	4.240	4.341	4.502	3.242	3.677	3.827	3.796	3.691	4.242	4.029
Na_2O	1.074	1.242	1.549	2.684	3.929	3.658	3.340	3.155	1.488	1.940	2.673	3.501	4.174	4.693	4.604
K_2O	5.437	4.152	2.988	1.960	0.952	0.444	0.230	0.126	5.899	4.599	3.097	1.794	0.914	0.372	0.127
H_2O	4.411	4.156	4.540	5.396	4.358	2.734	1.951	1.591	6.773	6.076	5.667	5.345	5.024	4.190	2.107
P	Eclogite melts - 5 kbar								Eclogite melts - 10 kbar						
T(°C)	778	859	915	946	969	988	1011	1037	807	866	931	996	1025	1046	1070
Melt	1st	2nd	3rd	4th	5th	6th	7th	8th	1st	2nd	3rd	4th	5th	6th	7th
SiO_2	70.836	65.582	57.949	54.229	52.499	51.685	51.429	51.403	66.991	66.875	62.322	54.381	51.374	50.092	49.464
Al_2O_3	12.476	13.535	13.588	12.816	12.370	12.208	12.306	12.500	14.077	14.204	14.732	13.549	12.677	12.374	12.363
FeO	1.087	5.420	12.647	17.233	19.196	19.728	19.302	18.513	0.960	2.582	6.981	16.712	20.747	22.105	22.311
MgO	0.206	1.147	3.123	4.766	5.931	6.854	7.535	8.123	0.165	0.497	1.550	4.128	5.562	6.461	7.174
CaO	1.901	2.100	2.046	2.057	2.127	2.234	2.403	2.625	2.165	2.345	2.404	2.370	2.447	2.595	2.789
Na_2O	3.810	5.143	5.950	5.759	5.542	5.403	5.394	5.417	4.403	4.907	5.842	5.735	5.256	4.958	4.762
K_2O	3.139	1.891	0.989	0.554	0.337	0.213	0.137	0.087	2.872	1.929	1.118	0.545	0.350	0.254	0.192
H_2O	6.545	5.183	3.710	2.586	1.998	1.674	1.494	1.333	8.367	6.663	5.051	2.581	1.587	1.162	0.945

*Melt compositions normalised without TiO_2 and O.

With increasing temperature the batches at 5 and 10 kbar progressively become more silica-poor (45–55 wt. %), and heavily so as quartz is consumed in the composition (by 850 °C at 5 kbar and 950 °C at 10 kbar). After quartz is exhausted the segregated melt fractions (6th to 8th) are less hydrous (1–3 wt. %), strongly enriched in FeO (17–23 wt. %) and MgO (6–9 wt. %), and moderately more calcic and sodic, with the higher T melt compositions shifting towards the CaO and MgO+FeO apices of the ternary plots (Table 5.1; Fig. 5.1b,c). The compositional changes observed with T in the segregated melts are very pronounced for those produced at lower P (5 kbar), whereas the compositional evolution is somewhat smoother and more gradual for melting at higher P (10 kbar). At 5 kbar, melt compositions vary from being granodioritic at 900 °C

to much more mafic gabbroic compositions by 1000 °C, whereas at higher P they only become dioritic at T exceeding 1000 °C (Fig. 5.1a,b,c).

5.2 Eclogite melt compositions

The batch melt compositions produced by the eclogite show similar trends in compositional space to that of the amphibolite, but with the absolute melt compositions controlled by the higher Na and lower K and Si content of the starting eclogite bulk composition (Table 5.1; Fig. 5.1). At both low P and high P, the eclogite compositions consistently plot at elevated Na_2O+K_2O values on the TAS relative to the amphibolite-derived batch melts at all temperatures.

At 5 kbar, the initial melt batches segregated below 800 °C (i.e. 1st and 2nd) are produced while quartz is present, and consequently they are siliceous (65–70 wt. %), hydrous (5–6.5 wt. %) and aluminous (12–14 wt. %) melts of broadly granitic chemistry (Table 5.1; Fig. 5.1a). The Na_2O content (3.8–5 wt. %) and K_2O content (1.8–3 wt. %) of the intial eclogite melts are higher and lower respectively than those for the early amphibolite melts (Fig. 5.1b). Similarly as identified for the amphibolite, the initial melt batches segregated below the temperature of quartz exhaustion (900 °C) at 10 kbar (1st to 3rd fractions) are silica-rich melts which are broadly granitic in composition, but are slightly less siliceous (66–67 wt. %), more aluminous (14–15 wt. %) and significantly more hydrous (6.5–8.5 wt. %) than those at 5 kbar (Table 5.1). All low-T melts contain only minor FeO and MgO (< 1 wt. % each).

Irrespective of pressure, beyond the T conditions at which quartz is consumed in the eclogite the calculated bulk chemistry of the segregated melt batches changes rapidly. The higher T melts (4th to 8th) become progressively depleted in SiO_2 (to as low as 49–51 wt. %) and H_2O (1–1.3 wt. %), very strongly enriched in FeO (up to 18–22 wt. %) and MgO (7–8 wt. %) and moderately more calcic (2.5–2.8 wt. %) and sodic (5–6 wt. %) melts of mafic composition (Table 5.1; Fig. 5.1b,c).

The changes in the compositional trends for the eclogite appear to be relatively smooth in comparison to those observed for the amphibolite, and this is likely due to quartz being consumed at lower T after only one or two melt batch segregations in the case of the eclogite. A consequence is that mafic melt compositions can potentially be generated at lower T for the eclogite bulk composition, with predominantly higher alkali monzodioritic to monzogabbroic melts produced above 900 °C at low-P (5 kbar) and above 1000 °C at high-P (10 kbar), as illustrated by Figs. 5.1a,b,c.

In summary, the compositional evolutionary trend of melt generated from the metabasic compositions appears to be (1) the generation of Si-rich, potassic granitic melts at near solidus low-T conditions in relatively minor proportions (1–3 vol. %) for only one or two batch segregations; (2) broadly granitic melt compositions, with varying Na_2O:K_2O ratios, appear to be generated at geologically-realistic temperatures for as long as quartz is available in the rock undergoing melting; and (3) the high-T melts, generated in the absence of quartz after its exhaustion in the rock, become rapidly more intermediate-to-mafic in composition and sequester FeO and MgO to a large extent. These melts that are generated at high fractions of melting have absolute compositions which may indeed resemble the tonalite and trondjhemite granitoids which were so prevalent during the Archean.

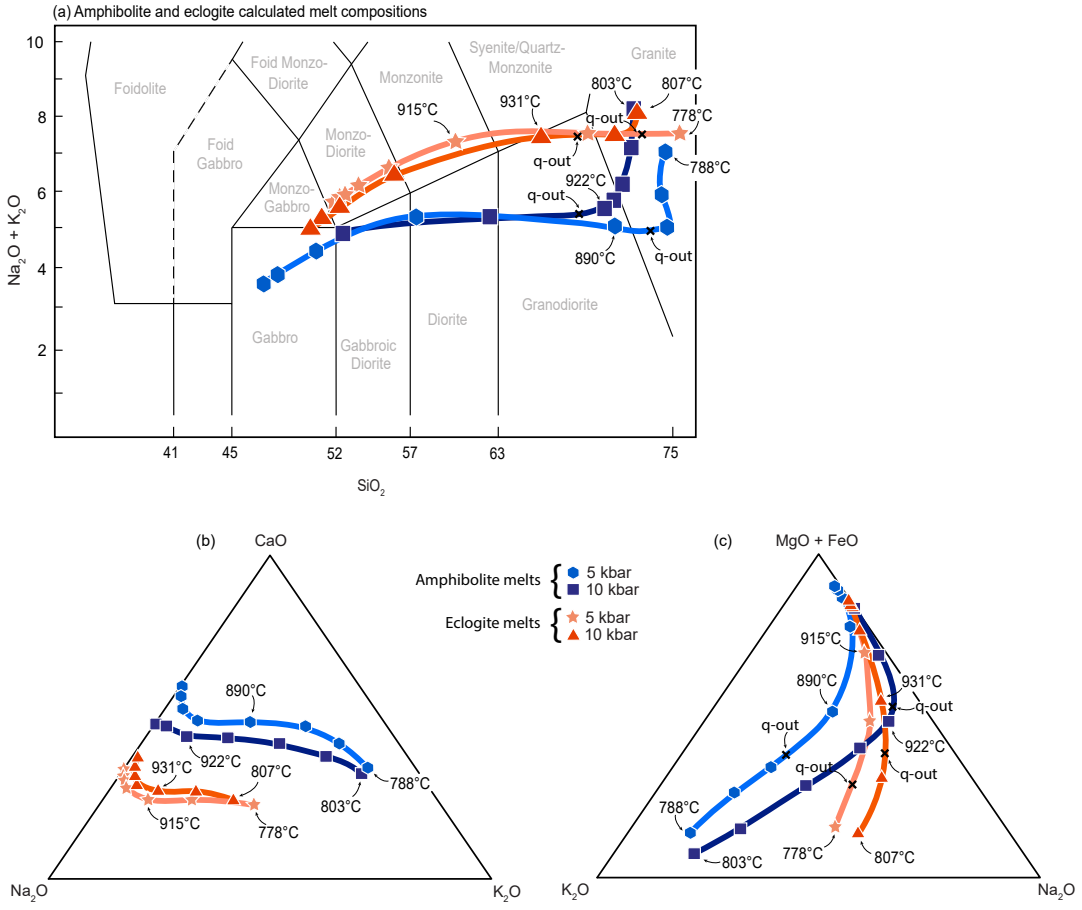

Figure 5.1: (a) Modified Total Alkali vs Silica (TAS) plot (Middlemost, 1994) for segregated melts produced from the amphibolite and eclogite at 5 and 10 kbar. (b) Ternary CaO–Na_2O–K_2O plot, showing the evolution of successive melt batches in ternary space. (c) Ternary (FeO+MgO)–Na_2O–K_2O plot for the calculated melt compositions

Chapter 6

Variations in bulk Si and T–$M_{\mathrm{SiO_2}}$ calculations

Quartz appears to exhibit a strong first-order influence on overall melt fertility of the metabasic compositions, the rate of melt production and the composition of the batch melts produced during open-system melting. In order to further elucidate the role of quartz in the melting process, a T–$M_{\mathrm{SiO_2}}$ section is constructed at 5 kbar for bulk SiO_2 varying from 45 to 55 mol. % for the amphibolite bulk composition (Fig. 6.1). The two normalised silica end-member bulk compositions used in the calculation are given in Table 3.2.

The T–$M_{\mathrm{SiO_2}}$ section in Fig. 6.1 has a relatively simple topology, with most of the lower-T suprasolidus equilibria and phase-in/out boundaries independant of Si content, or not strongly affected by it. The wet solidus occurs at 708 °C over the entire compositional range in bulk Si, augite is introduced into stable equilibrium at 730 °C, biotite is destabilised from the assemblage at 788 °C and orthopyroxene is introduced at around 820 °C for most contents of bulk Si. However, at bulk Si contents lower than 46 mol. %, orthopyroxene may stabilise to slightly higher T (up to 850–855 °C). The consumption of quartz in the rock occurs at 800 °C in low-Si compositions and is displaced to higher-T (880 °C) in high-Si compositions (Fig. 6.1). Hornblende is consumed at 860 °C for bulk compositions with greater Si contents, but persists to progressively higher T for compositions with lower Si contents. Hornblende is calculated to be present beyond the maximum modelled 1050 °C for SiO_2 contents below 47 mol. % (Fig. 6.1).

The closed-system melt proportion contours on the diagram have relatively shallow slopes at conditions between the wet solidus at 708 °C and the orthopyroxene-in boundary at 820 °C, with

melt production being essentially independant of Si content, and thus composition, at these conditions (Fig. 6.1). Around 10 vol. % melt is calculated to be produced over this interval before orthopyroxene stabilises, and anywhere between ∼15–30 vol. % melt may be accumulated before quartz-out, depending on the Si content of the rock.

Note that melt production becomes strongly focused where orthopyroxene, hornblende and quartz co-exist in stable equilibrium, and melting proceeds until quartz (for SiO_2 = 46–54 mol. %) or hornblende (for SiO_2 above 54 mol. %) is exhausted from the mineral assemblage. Up to 20–22 vol. % melt is calculated to be generated over less than a 50 °C interval by this assemblage (Fig. 6.1). The rate of melting slows dramatically once quartz is depleted from the rock and the contours attain a steeper slope in quartz-absent fields of the diagram. At these conditions, the absolute amount of melt produced becomes a function of both T and Si content of the metabasic composition.

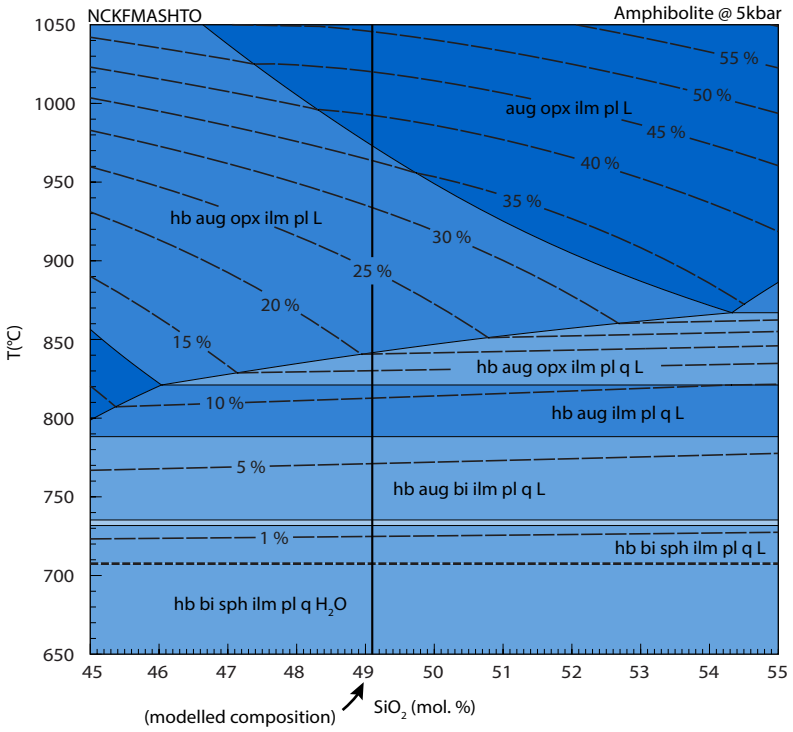

Figure 6.1: T–M_{SiO_2} section calculated for the amphibolite composition at 5 kbar, illustrating the effect of varying the bulk silica content on the suprasolidus phase equilbria and melt abundance. Bulk compositions used to construct the diagram are presented in Table 3.2

The effect of variation in bulk Si on open-system melting is demonstrated with modeboxes calculated for SiO_2 values of 45, 47, 49, 51, 53 and 55 mol. % (Fig. 6.2). Irrespective of Si value, the first melt batch is segregated at similar T in all compositions (780–790 °C), but the number of subsequent melt build up and batch segregation events between 830–880 °C is strongly dependent on the Si content of the rock. For example, in low-Si compositions (Fig. 6.2a,b), only a single melt batch is segregated over this 50 °C interval in T, whereas in Si-rich compositions (Fig. 6.2c–f) up to five rapid batch melt segregations may occur before 880 °C.

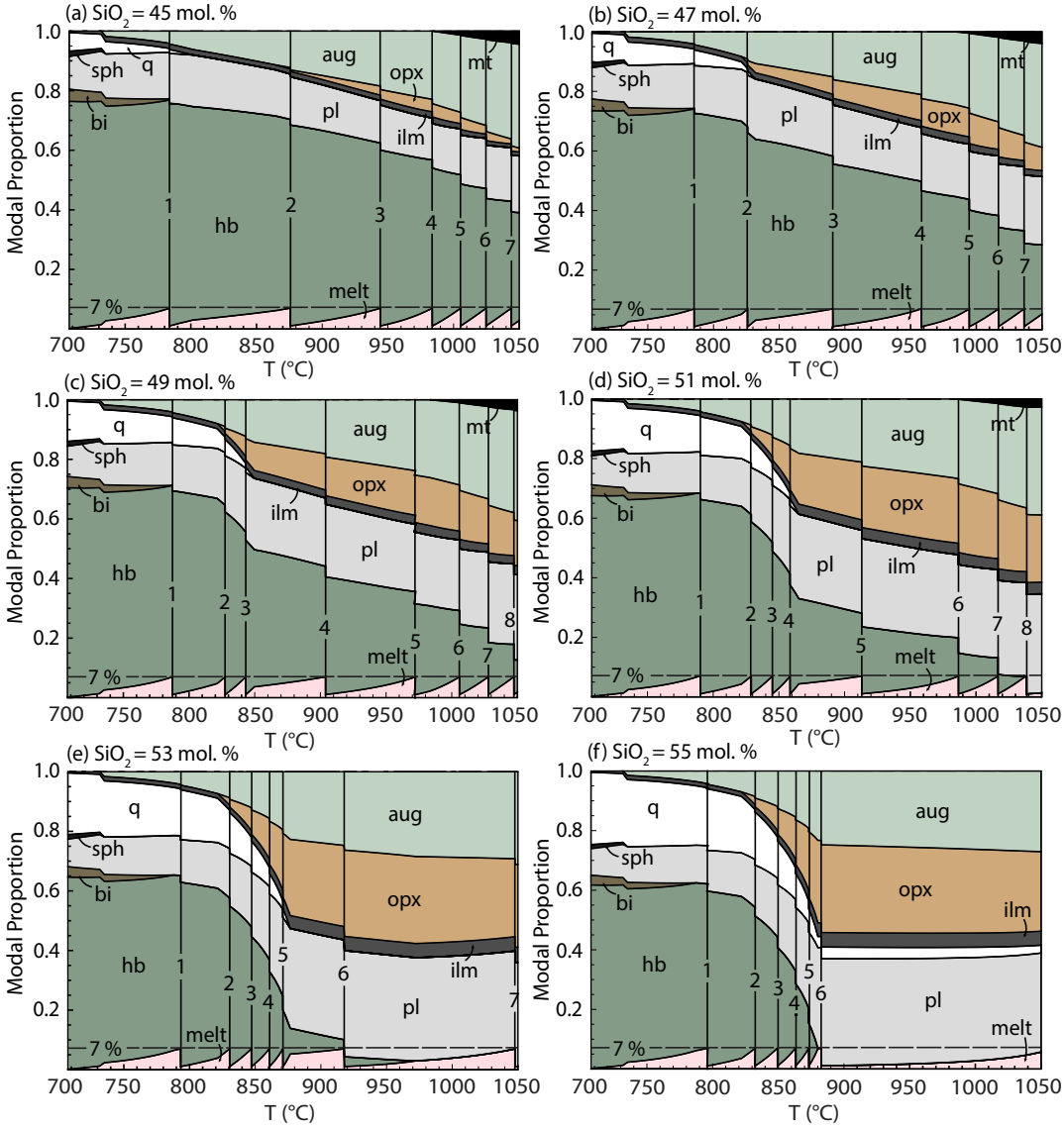

Figure 6.2: Modeboxes showing mineral abundance as a function of T at 5 kbar for the amphibolite composition with variable SiO_2 content. Diagrams are calculated for (a) Si = 45 mol. % (b) Si = 47 mol. % (c) Si = 49 mol. % (d) Si = 51 mol. % (e) Si = 53 mol. % and (f) Si = 55 mol. %

How many segregations happen before 880 °C depends on (1) whether quartz and orthopyroxene coexist; and (2) over what interval in T they coexist in stable equilibrium. For (2), the duration in T that they coexist is dependant on the proportion of quartz in the rock. In low-Si compositions, quartz is not abundant and may never be in equilibrium with orthopyroxene, and thus does not produce any significant melt (10–14 vol. %) by geologically-realistic T - 20–25 vol. % may instead be considered reasonable, but low-Si compositions do not generate these proportions in the modelling. Si-rich compositions see orthopyroxene introduced well before quartz is exhausted, after which quartz tends to be rapidly consumed alongside hornblende to produce large amounts of melt, calculated to be up to 35–40 vol. % in very Si-saturated compositions (Fig. 6.2e,f).

The low-Si compositions are rather modelled to produce significant proportions of melt above 900 °C (Fig. 6.2a–c), where high-T hornblende breakdown is significant, and rapid batch segregation may be envisaged for these high T. Si-rich compositions are extremely infertile at these T (Fig. 6.2e,f). This is likely due to all the hornblende in Si-rich compositions being rapidly consumed at low T such that it is exhausted by 900–950 °C and is a limiting phase during forward reaction progress to produce melt (Fig. 6.2e,f). Hornblende is more gradually consumed in Si-poor compositions and persists above 1050 °C (Fig. 6.2a–c).

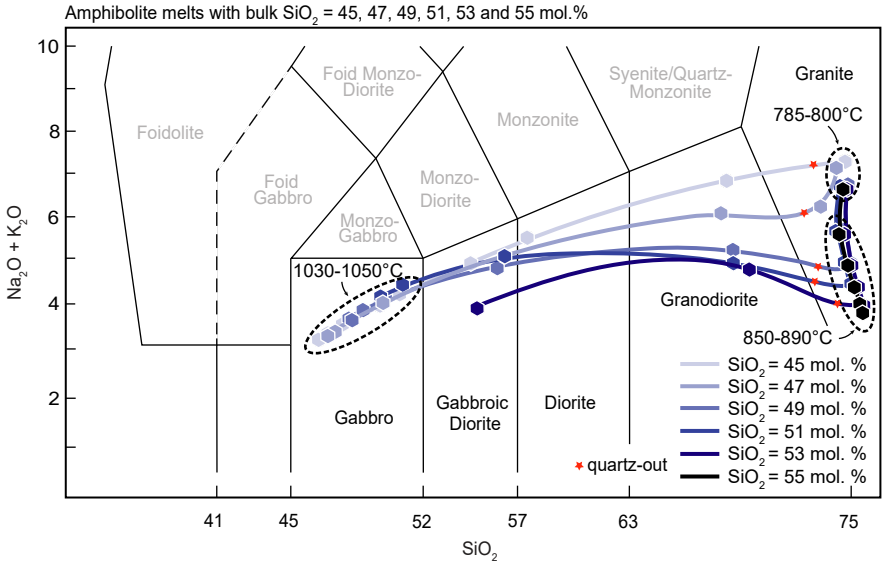

Figure 6.3: TAS compositional plot for the melts produced at 5 kbar from the amphibolite composition with variable SiO_2 content

The composition of progressive melt batches for variation in bulk Si are calculated at 5 kbar (Table 6.1). The melt evolution shows the same principal trends as for the original amphibolite and eclogite melt compositions.

Table 6.1: Melt batch compositions calculated for open-system melting at 5 kbar for the amphibolite bulk composition with variable SiO_2 content (normalised* wt. % oxide)

	45 mol. % SiO_2								47 mol. % SiO_2							
T(°C)	784	876	944	984	1005	1025	1044	1064	785	826	891	958	995	1017	1036	1056
Melt	1^{st}	2^{nd}	3^{rd}	4^{th}	5^{th}	6^{th}	7^{th}	8^{th}	1^{st}	2^{nd}	3^{rd}	4^{th}	5^{th}	6^{th}	7^{th}	8^{th}
SiO_2	71.774	65.012	54.900	48.582	46.718	46.012	45.795	45.798	71.771	71.819	64.692	54.262	48.889	47.162	46.504	46.295
Al_2O_3	13.060	14.726	15.327	14.541	14.172	14.042	14.054	14.152	13.074	12.938	14.548	14.978	14.137	13.774	13.672	13.713
FeO	0.797	4.394	12.386	19.416	21.383	21.784	21.438	20.705	0.826	1.723	4.890	13.434	19.540	21.297	21.561	21.129
MgO	0.148	0.908	2.934	5.062	6.235	7.153	7.972	8.759	0.153	0.324	1.085	3.440	5.546	6.769	7.713	8.547
CaO	3.158	4.029	4.797	5.165	5.276	5.341	5.405	5.486	3.171	3.598	4.177	4.639	4.807	4.893	4.968	5.055
Na_2O	1.093	1.847	2.470	2.337	2.334	2.409	2.519	2.634	1.082	1.210	2.334	3.083	2.962	2.916	2.940	2.992
K_2O	5.416	4.291	2.673	1.590	1.127	0.833	0.617	0.448	5.422	4.275	3.091	1.748	0.977	0.621	0.405	0.262
H_2O	4.553	4.794	4.514	3.307	2.755	2.425	2.200	2.019	4.500	4.113	5.184	4.415	3.141	2.568	2.237	2.008
	49 mol. % SiO_2								51 mol. % SiO_2							
T(°C)	787	828	843	904	973	1006	1028	1047	790	829	845	858	913	987	1017	1039
Melt	1^{st}	2^{nd}	3^{rd}	4^{th}	5^{th}	6^{th}	7^{th}	8^{th}	1^{st}	2^{nd}	3^{rd}	4^{th}	5^{th}	6^{th}	7^{th}	8^{th}
SiO_2	71.764	71.845	72.137	64.632	53.649	49.288	47.779	47.185	71.769	71.878	72.176	72.402	64.958	52.994	49.680	48.437
Al_2O_3	13.093	12.907	12.618	14.338	14.532	13.698	13.384	13.332	13.097	12.880	12.588	12.360	14.139	14.068	13.318	13.051
FeO	0.869	1.743	1.929	5.229	14.589	19.592	21.004	21.093	0.924	1.758	1.945	2.093	5.227	15.756	19.525	20.566
MgO	0.161	0.330	0.389	1.261	4.093	6.127	7.344	8.279	0.171	0.334	0.396	0.457	1.374	4.872	6.761	7.943
CaO	3.178	3.616	3.838	4.167	4.291	4.341	4.430	4.538	3.210	3.647	3.867	4.001	4.067	3.873	3.882	3.979
Na_2O	1.078	1.242	1.548	2.974	3.811	3.626	3.501	3.448	1.072	1.260	1.582	1.958	3.595	4.446	4.177	3.987
K_2O	5.434	4.162	3.003	1.945	0.941	0.475	0.261	0.143	5.384	4.050	2.866	1.825	1.013	0.397	0.173	0.075
H_2O	4.424	4.154	4.538	5.454	4.095	2.853	2.298	1.983	4.372	4.193	4.580	4.903	5.626	3.593	2.484	1.962
	53 mol. % SiO_2								55 mol. % SiO_2							
T(°C)	793	830	847	861	871	918	1048		797	832	849	863	873	883		
Melt	1^{st}	2^{nd}	3^{rd}	4^{th}	5^{th}	6^{th}	7^{th}		1^{st}	2^{nd}	3^{rd}	4^{th}	5^{th}	6^{th}		
SiO_2	71.770	71.900	72.204	72.425	72.566	65.747	54.002		71.785	71.938	72.250	72.470	72.608	72.708		
Al_2O_3	13.094	12.852	12.555	12.332	12.198	13.953	13.090		13.089	12.829	12.529	12.309	12.188	12.155		
FeO	0.985	1.778	1.970	2.115	2.186	4.829	17.852		1.043	1.793	1.984	2.120	2.174	2.202		
MgO	0.182	0.340	0.405	0.469	0.522	1.379	5.234		0.193	0.346	0.413	0.478	0.530	0.573		
CaO	3.229	3.659	3.878	4.005	4.054	3.924	4.288		3.271	3.692	3.909	4.026	4.065	4.095		
Na_2O	1.084	1.295	1.641	2.038	2.416	4.074	3.822		1.083	1.313	1.679	2.094	2.475	2.737		
K_2O	5.328	3.950	2.726	1.671	0.885	0.397	0.103		5.243	3.835	2.584	1.525	0.765	0.314		
H_2O	4.328	4.226	4.621	4.945	5.173	5.697	1.608		4.294	4.254	4.653	4.977	5.195	5.215		

*Melt compositions normalised without TiO_2 and O.

All initial melts are siliceous and hydrous, and are broadly granitic while generated in the presence of quartz in the rock. When quartz is depleted the melts become progressively more mafic and enriched in FeO+MgO, and the T that this happens depends on the amount of quartz present and not on the amount of melt already extracted, as Si-rich compositions rapidly produce five to six batches of granitic melt pre-900 °C before switching to insignificant mafic melt production, whereas Si-poor compositions begin to produce intermediate to mafic melts after only one or two segregations (Fig. 6.3).

Chapter 7

Residuum

Open-system melting has been shown to segregate significant proportions of melt from relatively fertile metabasic source rocks in this work. This efficient segregation will have an effect on the source rock from which the melt is extracted. To evaluate the consequences of melt loss on further melt productivity, two P–T pseudosections are calculated for melt-depleted, residuum compositions of amphibolite (Fig. 7.1a) and eclogite (Fig. 7.1b) after 3 high-P (10kbar) melt loss events at realistic orogenic temperatures (850–900 °C). Bulk compositions used in their construction are provided in Table 3.2.

Both residual P–T sections are characterised by high-grade, anhydrous mineral assemblages consisting of orthopyroxene at lower P and garnet at higher P. The only significant hydrous phase is biotite, which may be present below 650 °C (Fig. 7.1a). The major equilibria changes compared to the original closed-system (in-situ melting) pseudosection (Fig. 4.1a) are related to the orthopyroxene-in and garnet-in, with garnet-bearing assemblages stabilised to much lower P (4–5 kbar) at low temperatures approaching 600 °C, and orthopyroxene-bearing assemblages have drastically increased stability, and are stable up to 6 kbar at 600 °C. Rutile is present at high P above 7–8 kbar and ilmenite is stable at P below this.

Magnetite-bearing assemblages are stable at low P (2–4 kbar) for the drained amphibolite composition (Fig. 7.1a), but magnetite has increased stability in the eclogite, where it may persist to 6–8 kbar over the range in T, such that the magnetite, orthopyroxene and garnet can occur in stable equilibrium. Plagioclase persists up to 12 kbar in the eclogite (Fig. 7.1b), but destabilises at low T/high P conditions in the amphibolite.

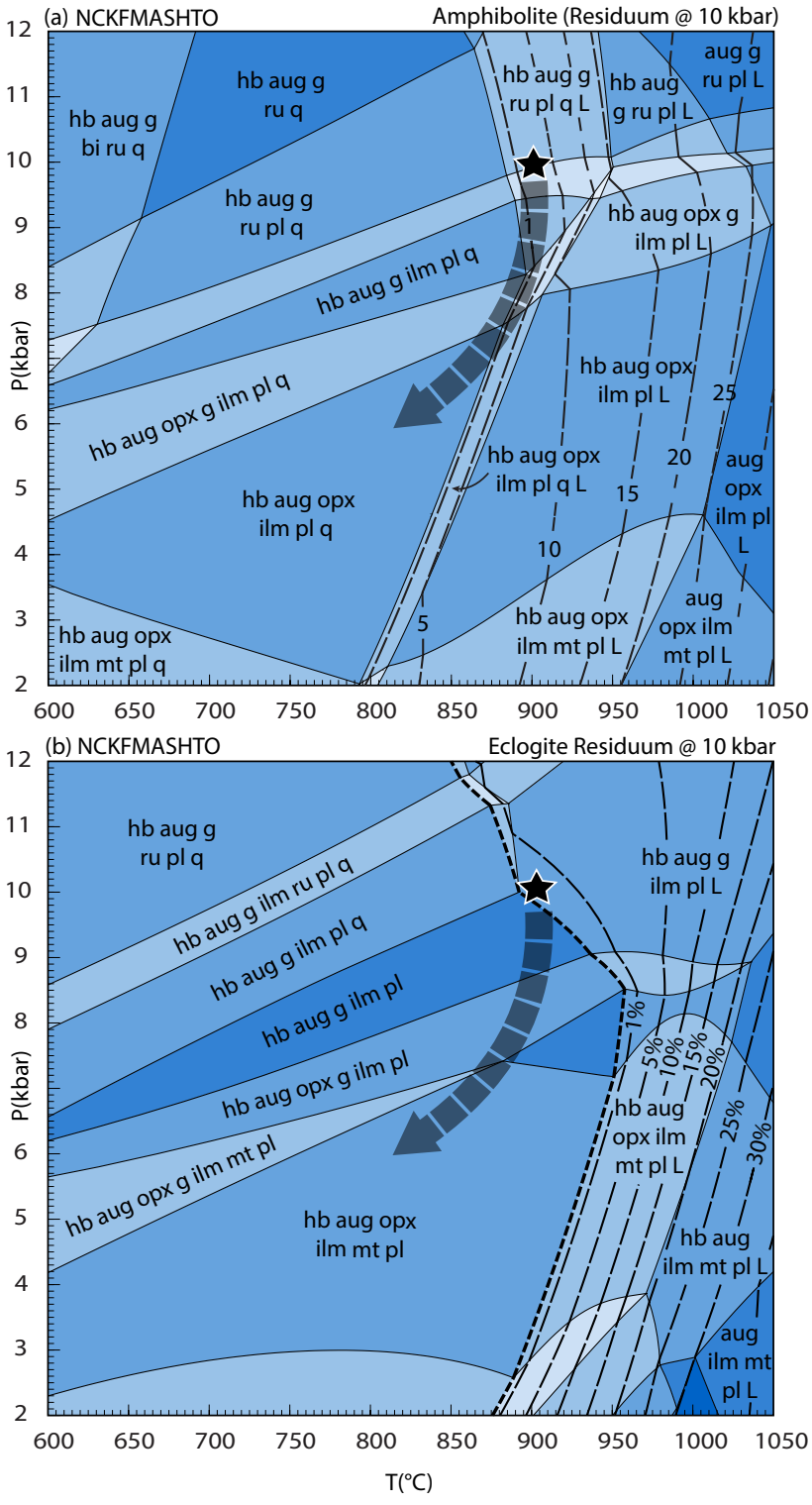

Figure 7.1: P–T sections calculated for the melt-depleted or 'drained' residuum compositions of amphibolite (a) and eclogite (b) after 3 melt loss events at 10 kbar. Black stars denote peak P–T_{max} conditions used for discussion purposes and arrows represent possible post-peak scenarios. Note the vastly increased P–T stability of two-pyroxene granulite

Hornblende is entirely consumed by 950 °C in the amphibolite at low-P and high-P conditions (Fig. 7.1a), but has extended stability to beyond 1050 °C in the eclogite, only being exhausted at around 1000 °C at low P. Conversely, orthopyroxene is exhausted in the eclogite by 900–1000 °C at low-to-intermediate P (Fig. 7.1b), but persists to well beyond 1050 °C in the melt-drained amphibolite composition.

In terms of P–T section topology, both diagrams show characteristic similarities, including a raised solidus which is elevated to the P–T conditions of melt segregation. The solidi in the residuum sections occur at 850–900 °C over the P range. The solidus has a negative slope (negative $\mathrm{d}P/\mathrm{d}T$) in higher P, garnet-bearing solidus fields and changes to a positive slope at the introduction of orthopyroxene to lower P. Melt abundance contours show the same consistent trend, with negative slopes in garnet-bearing fields and positive slopes in orthopyroxene stablity fields. Black star polygons indicate proposed peak P–T_{max} conditions at 10 kbar (880–900 °C) reached during a theoretical prograde metamorphic history and black, dashed arrows represent post-peak retrograde vectors of isothermal decompression and cooling encountered during exhumation.

The proposed P–T_{max} conditions are immediately to higher-T of the solidus, and the solid assemblage at these P–T conditions in the crust coexists with only a minor proportion of melt (1–3 vol. %). At lower crustal pressures (10 kbar), and considering the retrograde segments illustrated, the formerly melt-bearing equlibrium mineral assemblage in the rock would likely have crossed back over the solidus upon cooling almost immediately, with the bulk composition crystallising rapidly to a high-grade subsolidus assemblage dominated by ferromagnesian silicates.

Chapter 8

Discussion

8.1 Primary controls on melt productivity

It is well-established in the literature that dehydration melting and the subsequent breakdown of hydrous minerals in rocks presents a strong first-order control on voluminous melt production in the crust. Experimental and modelling contributions in metapelitic compositions(e.g. Thompson, 1982; Le Breton & Thompson, 1988; Patino-Douce & Johnston, 1991; Carrington & Harley, 1995; Greenfield *et al.*, 1998; White *et al.*, 2001, 2007; Yakymchuk & Brown, 2014) have demonstrated that the production of melt in these rocks is driven by the suprasolidus breakdown of H_2O-bearing muscovite at lower T, and biotite at higher T. The breakdown of these micas occurs through specific equilibria over a restricted range in P–T.

In mafic rocks neither muscovite, nor biotite is present in any significant proportion and consequently they do not exert a strong control on melt productivity. In these compositions, hornblende is instead the most voluminous hydrous phase, and both experimental and modelling contributions in mafic rocks (e.g. Beard & Lofgren, 1991; Wyllie & Wolf, 1993; Wolf & Wyllie, 1994; Green *et al.*, 2016; Palin *et al.*, 2016) has shown that hornblende breakdown, and thus melt production, appears to be much more continuous and gradual as a response to the multi-equilibria consumption of the amphibole over a significantly wider range in P–T (200–250 °C).

In the results of this modelling study, there is clear phase equilibria evidence that melt production in mafic compositions can be significantly focused, and the rate of melting can be drastically increased over a restricted P–T interval.

The equilibrium coexistence of hornblende, quartz and orthopyroxene in the mafic rock corresponds to a rapid increase in the melting rate, and this equilibria can be intersected along prograde P–T paths at low to intermediate P (4–8 kbar) at 820–880 °C, which is well within the realm of continental orogenic metamorphism. When this equilibria is first encountered, a stepped increase in melting rate may be observed at the onset of the following dehydration melting reaction

$$\text{hornblende} + \text{quartz} \pm \text{plagioclase} \pm \text{augite} = \text{orthopyroxene} + \text{melt} \pm \text{ilmenite} \tag{8.1}$$

This reaction appears to be important for generating voluminous melt from metamafic rocks at orogenic conditions in the crust, and broadly agrees with the amphibole breakdown reactions in experimental studies. The approximate stoichiometry in which hornblende and quartz are consumed in the melting reaction is 3:1, with hornblende consumed at thrice the rate of quartz, as previously noted by Hartel & Pattison (1996). Modal quartz is likely to be exhausted first by reaction (8.1) in most mafic rocks, but this will depend greatly on the SiO_2 content of the mafic composition and the abundance of quartz in the rock. A subsolidus quartz abundance of around 10 vol. % is required for reaction (8.1) to be crossed. At proportions below this, quartz will be exhausted by melting before orthopyroxene can be introduced into stable equilibrium (cf. Fig. 6.2) and focused melt production will not be realised. In terms of quantifying productivity, a typical mafic composition with around 15 vol. % quartz for example, will produce $\sim$ 20–22 vol. % melt through reaction (8.1) before quartz is depleted (cf. Fig. 6.2).

8.2 Controls on the composition of segregated melt batches

The subsolidus protolith composition of the mafic rock very strongly influences the composition of the derived partial melts, in particular, the Na/K ratio and the absolute alkali contents of the melts. Thus, depending on the bulk alkali ratio of the starting composition, different families of melt may be produced from a given mafic rock. For example, the eclogite composition modelled in this study is more Na-rich than it is K-rich and the bulk composition of the rock has a higher Na/K ratio, as well as higher overal alkali contents, compared to the amphibolite.

Consequently, the eclogite is observed to produce melt which is more sodic in character, and which has elevated Na + K. These melts define a granite–syenite/quartz-monzonite– monzonite–monzo-diorite–monzogabbro compositional trend (Fig. 5.1a). The amphibolite rather produced melts which are less sodic, lower in Na + K on the TAS and define a granite–granodiorite–diorite–gabbroic-diorite–gabbro compositional trend (Fig. 5.1a).

The metamafic bulk composition is thus broadly taken to be the first-order control on melt composition, and different rocks with even minor chemical differences from different orogenic localities will produce different melts. The results presented here also demonstrate that melts of significantly different composition can be generated from a single protolith bulk composition by successive extraction from the rock. However, the modelling here considers only the primary melt compositions produced and does not consider further modification of the melt compositions by fractional crystallization and/or peritectic mineral entrainment.

For example, at lower T, intial melting at the solidus occurs predominantly via the breakdown of biotite, which is large reservoir for potassium, and the early-formed melts are consequently a reflection of this, being K-rich and granitic in composition. Once biotite has been completely consumed in the rock, incongruent dehydration melting instead progressively consumes hornblende, and the input of K into the generated melts is no longer significant, as Na is increasingly favoured. This defines an increase in the Na/K ratio and more tonalitic-trondhjemitic melts are produced out of the same protolith. Thus, given a specific rock, the T at which melting and segregation occurs, and by extension the hydrous phase which is broken down at that T, exerts further control on the melt composition.

Additionally, it is demonstrated here that for as long as quartz is present in the metamafic rock, the melts produced and segregated are broadly granitic in composition. SiO_2 is strongly incorporated into the melt through the progressive consumption of quartz, and the more quartz (and, thus SiO_2) is available, the longer more silica-rich granitic melt will be produced. The main variation in broadly granite melt chemistry is rather manifested in the changing ratios of the alkali elements. However, the introduction of orthopyroxene to the rock catalyses the exhaustion of quartz, and when this happens at a given T through reaction (8.1), the melts produced thereafter are no longer granitic, but considerably more low-Si, mafic melts with highly elevated Fe + Mg contents.

8.3 The volume and composition of melt produced during open-system orogenic anatexis

The results here, as well as the above sections, have established that bulk SiO_2 in the protolith plays an important role in determining both the composition and amount of melt produced during orogenic anatexis, and that conditions where quartz runs out triggers significant changes in both

melt fertility of the rock, as well as melt composition. For many mafic compositions, quartz will be depleted through reaction (8.1) at T conditions of 820–880 °C in the orogenic crust, with all the derived melt produced up to that point being broadly granitic in composition. At these P–T conditions, on the order of 20 vol. % melt may be produced from mafic compositions containing ∼50 mol. % SiO_2 (∼15 vol. % free quartz). This is sufficient melt for multiple segregation and extraction events to occur during orogenesis.

In terms of bulk Si variation, more Si-rich mafic rocks will produce higher volumes of granite melt than Si-poor rocks at the same P–T conditions during metamorphism, and would appear to be much more fertile. Conversely, Si-poor rocks are much less fertile at these attainable T conditions as quartz in the rock is exhausted before orthopyroxene can be stabilised in any significant proportion to boost the production of melt (and fertility) of the rock. In such low-Si rocks, it is likely that only enough melt for one or two segregations will be produced by 900 °C, and temperatures beyond this are not commonly attained. The first melt segregation will likely have a K-rich granitic to syenitic composition. Following this, only low volumes (5–10 vol. %) of more mafic granodioritic to dioritic melt would be further produced at T below 900 °C.

Notably while being reasonably fertile at T below 900 °C, high-Si compositions can become very infertile and refractory at T above this, the reason being chiefly because most of the hornblende that was present in the rock has already been exhausted by these conditions and the melt fertility is minimal. These compositions will therefore only produce very minor amounts (7–10 vol. %) of more intermediate to mafic melts at conditions approaching those of UHT metamorphism in the orogenic continental crust. By contrast, at UHT conditions, low-Si compositions may be significantly more fertile, as hornblende in these rocks can persist to these high T and remain relatively unmelted. In such Si-depleted lithologies, around 20 vol. % dioritic to gabbroic melt may be produced between 900 and 1000 °C.

Given the above, even though the volume and composition of melt derived from mafic lithologies depends on the alkali and silica content of the protolith, the open-system melting behaviour of these lithologies under typical orogenic P–T is likely to yield around 20 vol. % of granite melt only. UHT crustal conditions are likely required to generate meaningful volumes of more intermediate to mafic melt. This amount of melt suggested to be derived from the mafic protolith above is more than sufficient to undergo segregation and contribute to granite magmatism in the upper crust.

Furthermore, while metapelitic lithologies have been calculated to be exceedingly fertile for melt generation (35–45 vol. %) at similar P–T conditions (e.g. White *et al.*, 2001; White & Powell, 2002; Yakymchuk & Brown, 2014), they are a relatively minor component of the mid-to-lower crust, and therefore the contribution of mafic rocks to granite magmatism and internal crustal differentation should not be underestimated. Similarly, other non-pelitic sources (e.g. metagranitoids) may also generate broadly granitic melts which undoubtedly contribute to upper-level granite emplacement (e.g. Jung *et al.*, 2000).

8.4 Consequences of open-system melting

Regardless of the amount of melt segregated and extracted from the rock, the net effect of melt loss is to inhibit further melt fertility. However, the extraction of larger volumes will amplify the effects. When melt is extracted and the bulk composition fractionated, the new solidus for the depleted bulk composition is elevated to the P–T conditions of extraction (see Fig. 7.1a, b), and further extraction will further raise the solidus T (White & Powell, 2002). Thus after each melt loss event, to melt the rock further requires increasingly greater temperatures in the crust to segregate additional melt. These temperatures are likely not easily attainable in the majority of orogenies, and usually require considerable thermal input in the form of mantle influence, for example.

Furthermore, the drained compositions have increased stability range of two-pyroxene granulite assemblages. Melt loss carries away both H_2O and the alkalis from the source, and these are essential components for facilitating rehydrating back reactions between the melt and the residual minerals to lower the grade of the assemblage upon retrogression. If the melt is lost then this will not happen, and the granulite-grade mineral assemblage will persist in the rock as it cools. Therefore the additional effect of melt loss is to increase the preservation potential of granulite-facies assemblages (see White & Powell (2002) for a comprehensive discussion). The residuum is comprised of a strong garnet-pyroxene framework after melt has been lost, and this may have the rheologic effect of strengthening the solid fraction of the crust, and creating a dry, elastic lower crust (e.g. Diener & Fagereng, 2014).

If the P–T_{max} points in Fig. 7.1a, b are considered and isothermal decompression and cooling occur during exhumation then the negatively-sloped topology of the solidus may mean that the

rock could remain melt-bearing for a limited period of time before becoming subsolidus, but given that the solid assemblage will only coexist with 1–3 vol. % melt at the maximum P–T of metamorphism, and the peak conditions are very close to the raised solidus, the bulk composition should cool almost immediately to the anhydrous granulite assemblage dominated by ferromagnesian sillicates. The very minor proportion of melt is considered to be insignificant and does not play a prominent role in retrogression.

Additionally, the negative slope of the melt contours on Fig. 7.1a, b imply that no further melting will occur as P is lowered, and decompression melting in these mafic compositions is therefore not likely. This is importantly in agreement with Yakymchuk & Brown (2014) who concluded that decompression melting in their metapelitic compositions was unlikely and did not contribute to buoyancy during exhumation.

Chapter 9

Conclusions

The metamafic lithologies modelled here appear to produce a volumetrically significant amount of melt under orogenic conditions, and are therefore viable and fertile source rocks for generating granitoid melts. The generation of melt occurs continuously through the fluid-absent decomposition of hornblende over a wide range in suprasolidus P–T of around 200–250 °C. However, the obtained results have demonstrated that melt production can be significantly focused at the conditions where orthopyroxene coexists with hornblende and quartz at low-to-intermediate P. The majority of melt in these rocks appears to be produced between 820 and 880 °C at this P, and the generation of the melt will most likely be limited by quartz. Once quartz has been depleted only small volumes of more intermediate to mafic composition are generated at UHT conditions.

The proportion of melt generated from these compositions is around half of that produced from a metapelite at similar P–T, and while mafic rocks may appear significantly less fertile than pelites, they have the potential to make a meaningful contribution to crustal differentiation. Whereas the role of mafic anatexis is unequivocal for the generation of continental crust in the Archaean (e.g. Foley *et al.*, 2002; Martin & Moyen, 2002; Rapp *et al.*, 2003; Moyen & Stevens, 2006; Moyen & Martin, 2012), it however does not readily appear to be greatly recognised in the geochemical signature of Proterozoic and Phanerozoic orogenic granites. This apparent discrepancy may be due to under-reporting because of a perception that mafic lithologies are not viable fertile source rocks for modern orogenic granitic melts, such that hornblende does not play a prominent role in the genesis of modern granite (e.g. Martin, 1986). Alternatively, it may be that the generated melts do not contribute to crustal differentiation by, for example, being largely retained in the near-source region.

The physical mechanisms of melt segregation and migration have been described for metapelites and associated rock types (Sawyer, 1994, 2001; Brown & Solar, 1998a,b; Weinberg, 1999; Kisters *et al.*, 2009), but their applicability to mafic rocks has not been tested. It is possible that mesoscale melt extraction from mafic rocks may be more difficult or less efficient due to, for example, the granular textural characteristic of the parental basalt, and consequent lack of an interconnected mica fabric that facilitates leucosome formation (Sawyer, 2001), or because mafic units are typically more competent and may therefore become areas of mesoscale melt accumulation rather than melt loss (e.g. Diener *et al.*, 2014).

Additionally, the segregation of increasingly more mafic melts from these rocks may be hindered given the density contrast between the tonalite-trondhjemite melt and the mafic residue, which may be less than that for a comparable pelite host and haplogranite melt. This segregation potential is partly dependant on the viscosity of the melt, which in turn is dependant on melt H_2O content (Rapp *et al.*, 1991). Thus the early-formed, hydrous granite melts calculated to be produced here are suggested to have reduced viscosity and may assume a high segregation potential to contribute to granite magmatism, whereas this may not be as significant for less hydrous, and more viscous tonalite-trondhjemite melt.

The modelling work presented here has thus utilised appropriate bulk compositions to quantify, constrain and address a few knowledge gaps regarding open-system melting in metamafic rocks, and presents some further progress into modelling high-T processes in these metamorphosed compositions. The effects of melt loss have been examined and principle controls on the melt compositions and melt evolution have been established. That bulk silica content and the stable equilibrium of orthopyroxene and quartz play such a prominent role in the suprasolidus evolution of metamafic rocks, and their derived melts, represents a significant initial platform from which to further investigate the high-grade processes in deep, lower crust using mineral equilibria modelling methods.

References

Afonso, J. C. & Ranalli, G., 2004. Crustal and mantle strengths in the continental lithosphere: Is the jelly sandwich model obsolete? *Tectonophysics*, **394**, 221–232.

Ague, J. J., 1991. Evidence for major mass-transfer and volume strain during regional metamorphism of pelites. *Geology*, **19**, 855–858.

Arndt, N. T. & Christensen, U., 1992. The role of lithospheric mantle in continental flood volcanism: thermal and geochemical constraints. *Journal of Geophysical Research: Solid Earth*, **97**(B7), 10967–10981.

Beard, J. S. & Lofgren, G. E., 1991. Dehydration melting and water-saturated melting of basaltic and andesitic greenstones and amphibolites at 1, 3 and 6–9 kb. *Journal of Petrology*, **32**(2), 365–401.

Brown, M., 2001. Orogeny, migmatites and leucogranites: a review. *Journal of Earth System Science*, **110**(4), 313–336.

Brown, M., 2002. Retrograde processes in migmatites and granulites revisited. *Journal of Metamorphic Geology*, **20**, 25–40.

Brown, M., 2004. The mechanism of melt extraction from the lower continental crust of orogens. *Transactions of the Royal Society of Edinburgh*, **95**, 35 – 48.

Brown, M., 2007a. Crustal melting and melt extraction, ascent and emplacement in orogens: mechanisms and consequences. *Journal of the Geological Society*, **164**, 709 – 730.

Brown, M., 2007b. Metamorphic conditions in orogenic belts: a record of secular change. *International Geology Review*, **49**, 193–134.

Brown, M., 2010. The spatial and temporal patterning of the deep crust and implications for the process of melt extraction. *Philosophical Transactions of the Royal Society of London, Series A*, **368**, 11 – 51.

Brown, M. & Solar, G. S., 1998a. Granite ascent and emplacement during contractional deformation in convergent orogens. *Journal of Structural Geology*, **20**, 1365–1393.

Brown, M. & Solar, G. S., 1998b. Shear-zone systems and melts: feedback relations and self-organization in orogenic belts. *Journal of Structural Geology*, **20**, 211–227.

Brown, M. & Solar, G. S., 1999. The mechanism of ascent and emplacement of granite magma during transpression: a syntectonic granite paradigm. *Tectonophysics*, **312**, 1–33.

Brown, M. A., Brown, M., Carlson, W. D. & Denison, C., 1999. Topology of syntectonic melt-flow networks in the deep-crust: Inferences from three-dimensional images of leucosome geometry in migmatites. *American Mineralogist*, **84**, 1793–1818.

Brown, M., Averkin, Y. A., McLellan, E. L. & Sawyer, E. W., 1995. Melt segregation in migmatites. *Journal of Geophysical Research: Solid Earth*, **100**(B8), 15655–15679.

Brown, M., Korhonen, F. J. & Siddoway, C. S., 2011. Organizing melt flow through the crust. *Elements*, **7**, 261–266.

Cagnard, F., Gapais, D. & Barbey, P., 2007. Collision tectonics involving juvenile crust: the sample of the southern Svecofennides. *Precambrian Research*, **154**, 125–141.

Carrington, D. & Harley, S., 1995. Partial melting and phase relations in high-grade metapelites: an experimental petrogenetic grid in the KFMASH system. *Contributions to Mineralogy and Petrology*, **120**(3-4), 270–291.

Christensen, N. I. & Mooney, W. D., 1995. Seismic velocity structure and composition of the continental crust: A global view. *Journal of Geophysical Research: Solid Earth*, **100**(B6), 9761–9788.

Clark, C., Fitzsimons, I. C. W., Healy, D. & Harley, S. L., 2011. How does the continental crust get really hot? *Elements*, **7**, 235–240.

Clemens, J. & Vielzeuf, D., 1987. Constraints on melting and magma production in the crust. *Earth and Planetary Science Letters*, **86**(2), 287–306.

Clemens, J. D., 1990. The Granulite-Granite Connexion. *Granulites and Crustal Evolution*, **311**, 25–36.

Clemens, J. D., 2006. Melting of the continental crust: fluid regimes, melting reactions, and source-rock fertility, *Evolution and Differentiation of the Continental Crust*, pp. 296–330. Cambridge University Press.

Condie, K. C., 1989. Geochemical changes in basalts and andesites across the Archean-Proterozoic boundary: Identification and significance. *Lithos*, **23**(1), 1–18.

Condie, K. C., 1993. Chemical composition and evolution of the upper continental crust: contrasting results from surface samples and shales. *Chemical geology*, **104**(1), 1–37.

Condie, K. C., 1999. Mafic crustal xenoliths and the origin of the lower continental crust. *Lithos*, **46**(1), 95–101.

Dewey, J. F. & Windley, B. F., 1981. Growth and differentiation of the continental crust. *Philosophical Transactions of the Royal Society of London A: Mathematical, Physical and Engineering Sciences*, **301**(1461), 189–206.

Diener, J. F. A. & Fagereng, Å., 2014. The influence of melting and melt drainage on crustal rheology during orogenesis. *Journal of Geophysical Research: Solid Earth*, **119**(8), 6193–6210.

Diener, J. F. A., White, R. W. & Hudson, T. J. M., 2014. Melt production, redistribution and accumulation in mid-crustal source rocks, with implications for crustal-scale melt transfer. *Lithos*, **200–201**, 212–225.

Diener, J. F. A., White, R. W., Link, K., Dreyer, T. S. & Moodley, A., 2013. Clockwise, low-P metamorphism of the Aus granulite terrain, Southern Namibia, during the Mesoproterozoic Namaqua Orogeny. *Precambrian Research*, **224**, 629–652.

Downes, H., 1993. The nature of the lower continental crust of Europe: petrological and geochemical evidence from xenoliths. *Physics of the earth and planetary interiors*, **79**(1), 195–218.

Drummond, M. & Defant, M., 1990. A model for trondhjemite-tonalite-dacite genesis and crustal growth via slab melting: Archean to modern comparisons.. *Journal of Geophysical Research: Solid Earth*, **95**(B13), 21503–21521.

England, P. C. & Thompson, A. B., 1984. Pressure-Temperature-time paths of regional metamorphism I. Heat transfer during the evolution of regions of thickened continental crust. *Journal of Petrology*, **25**(4), 894–928.

England, P. C. & Thompson, A. B., 1986. Some thermal and tectonic models for crustal melting in continental collision zones. *Geological Society, London, Special Publications*, **19**(1), 83–94.

Foley, S., Tiepolo, M. & Vannucci, R., 2002. Growth of early continental crust controlled by melting of amphibolite in subduction zones. *Nature*, **417**(6891), 837–840.

Gallagher, K. & Hawkesworth, C., 1992. Dehydration melting and the generation of continental flood basalts. *Nature*, **358**(6381), 57–59.

Green, E. C. R., Holland, T. J. B. & Powell, R., 2007. An order–disorder model for omphacitic pyroxenes in the system jadeite–diopside–hedenbergite–acmite, with applications to eclogitic rocks. *American Mineralogist*, **92**, 1181–1189.

Green, E. C. R., White, R. W., Diener, J. F. A., Powell, R., Holland, T. J. B. & Palin, R. M., 2016. Activity-composition relations for the calculation of partial melting equilibria in metabasic rocks. *Journal of Metamorphic Geology*, DOI:10.1111/jmg.12211.

Green, T., 1976. Experimental generation of cordierite-or garnet-bearing granitic liquids from a pelitic composition. *Geology*, **4**(2), 85–88.

Greenfield, J. E., Clarke, G. L. & White, R. W., 1998. A sequence of partial melting reactions at Mt Stafford, central Australia. *Journal of Metamorphic Geology*, **16**, 363–378.

Grosch, E. G., Bisnath, A., Frimmel, H. E. & Board, W. S., 2007. Geochemistry and tectonic setting of mafic rocks in western Dronning Maud Land, East Antarctica: implications for the geodynamic evolution of the Proterozoic Maud Belt. *Journal of the Geological Society*, **164**(2), 465–475.

Handy, M. R., Mulch, A., Rosenau, M. & Rosenberg, C. L., 2001. The role of fault zone and melts as agents of weakening, hardening and differentiation of the continental crust: a synthesis, *Nature and tectonic significance of fault zone weakening*, Vol. 186, pp. 305–332. Geological Society of London Special Publication.

Harley, S. L., 1988. Proterozoic granulites from the Rauer Group, East Antarctica. I. Decompressional pressure-temperature paths deduced from mafic and felsic gneisses. *Journal of Petrology*, **29**(5), 1059–1095.

Harley, S. L., 1998. On the occurrence and characterization of Ultrahigh-Temperature (UHT) crustal metamorphism. *Geological Society, London, Special Publications*, **138**(1), 81–107.

Harris, N. & Inger, S., 1992. Trace element modelling of pelite-derived granites. *Contributions to Mineralogy and Petrology*, **110**(1), 46–56.

Hartel, T. & Pattison, D., 1996. Genesis of the Kapuskasing (Ontario) migmatitic mafic granulites by dehydration melting of amphibolite: the importance of quartz to reaction progress. *Journal of Metamorphic Geology*, **14**(5), 591–611.

Helz, R. T., 1976. Phase relations of basalts in their melting ranges at PH_2O = 5 kb. Part II. Melt compositions. *Journal of Petrology*, **17**(2), 139–193.

Holland, T. & Powell, R., 2001. Calculation of phase relations involving haplogranitic melts using an internally consistent thermodynamic dataset. *Journal of Petrology*, **42**(4), 673–683.

Holland, T. J. B. & Powell, R., 2011. An improved and extended internally consistent thermodynamic dataset for phases of petrological interest, involving a new equation of state for solids. *Journal of Metamorphic Geology*, **29**, 333–383.

Holloway, J. & Burnham, C. W., 1972. Melting relations of basalt with equilibrium water pressure less than total pressure. *Journal of Petrology*, **13**(1), 1–29.

Humphris, S. E. & Thompson, G., 1978. Hydrothermal alteration of oceanic basalts by seawater. *Geochimica et Cosmochimica Acta*, **42**(1), 107–125.

Jackson, S. E., Pearson, N. J., Griffin, W. L. & Belousova, E. A., 2004. The application of laser ablation-inductively coupled plasma mass spectrometry to in situ U–Pb zircon geochronology. *Chemical Geology*, **211**, 47–69.

Jahn, B., Liu, X., Yui, T., Morin, N. & Bouhnik-Le Coz, M., 2005. High-pressure/ultrahigh-pressure eclogites from the Hongan Block, East-Central China: geochemical characterization, isotope disequilibrium and geochronological controversy. *Contributions to Mineralogy and Petrology*, **149**(5), 499–526.

Janoušek, V., Farrow, C. & Erban, V., 2006. Interpretation of whole-rock geochemical data in igneous geochemistry: introducing Geochemical Data Toolkit (GCDkit). *Journal of Petrology*, **47**(6), 1255–1259.

Johannes, W. & Holtz, F., 1996. The tonalite system Qz-Ab-An, *Petrogenesis and experimental petrology of granitic rocks*, pp. 202–228. Springer.

Johnson, T. E., Brown, M., Kaus, B. J. & VanTongeren, J. A., 2014. Delamination and recycling of Archaean crust caused by gravitational instabilities. *Nature Geoscience*, **7**(1), 47–52.

Johnson, T. E., White, R. W. & Powell, R., 2008. Partial melting of metagreywacke: a calculated mineral equilibria study. *Journal of Metamorphic Geology*, **26**, 837–853.

Johnson, T., Fischer, S., White, R., Brown, M. & Rollinson, H., 2012. Archaean intracrustal differentiation from partial melting of metagabbrofield and geochemical evidence from the central region of the Lewisian complex, NW Scotland. *Journal of Petrology*, **53**(10), 2115–2138.

Jung, S., Hoernes, S. & Mezger, K., 2000. Geochronology and petrogenesis of Pan-African, syntectonic, S-type and post-tectonic A-type granite (Namibia): products of melting of crustal sources, fractional crystallization and wall rock entrainment. *Lithos*, **50**(4), 259–287.

Jung, S., Hoernes, S. & Mezger, K., 2002. Synorogenic melting of mafic lower crust: constraints from geochronology, petrology and Sr, Nd, Pb and O isotope geochemistry of quartz diorites (Damara Orogen, Namibia). *Contributions to Mineralogy and Petrology*, **143**, 551 – 566.

Kemp, A., Hawkesworth, C., Foster, G., Paterson, B., Woodhead, J., Hergt, J., Gray, C. & Whitehouse, M., 2007. Magmatic and crustal differentiation history of granitic rocks from Hf–O isotopes in zircon. *Science*, **315**(5814), 980–983.

Kisters, A. F. M., Ward, R. A., Anthonissen, C. J. & Vietze, M. E., 2009. Melt segregation and far-field melt transfer in the mid-crust. *Journal of the Geological Society, London*, **166**, 905–918.

Korhonen, F. J., Saito, S., Brown, M. & Siddoway, C. S., 2010. Modelling multiple melt loss events in the evolution of an active continental margin. *Lithos*, **116**, 230–248.

Laporte, D. & Watson, E. B., 1995. Experimental and theoretical constraints on melt distribution in crustal sources: the effect of crystalline anisotropy on melt interconnectivity. *Chemical Geology*, **124**(3), 161–184.

Laporte, D., Rapaille, C. & Provost, A., 1997. Wetting angles, equilibrium melt geometry, and the permeability threshold of partially molten crustal protoliths, *Granite: From Segregation of Melt to Emplacement Fabrics*, pp. 31–54. Kluver Academic Publishers.

Le Bas, M. J., Le Maitre, R., Streckeisen, A., Zanettin, B.et al., 1986. A chemical classification of volcanic rocks based on the total alkali-silica diagram. *Journal of petrology*, **27**(3), 745–750.

Le Breton, N. & Thompson, A. B., 1988. Fluid-absent (dehydration) melting of biotite in metapelites in the early stages of crustal anatexis. *Contributions to Mineralogy and Petrology*, **99**(2), 226–237.

Li, X. H., Sun, M., Wei, G., Liu, Y., Lee, C. & Malpas, J., 2000. Geochemical and Sm–Nd isotopic study of amphibolites in the Cathaysia Block, Southeastern China: evidence for an extremely depleted mantle in the Paleoproterozoic. *Precambrian Research*, **102**(3), 251–262.

López, S. & Castro, A., 2001. Determination of the fluid–absent solidus and supersolidus phase relationships of morb-derived amphibolites in the range 4–14 kbar. *American Mineralogist*, **86**(11-12), 1396–1403.

Lustrino, M., 2005. How the delamination and detachment of lower crust can influence basaltic magmatism. *Earth-Science Reviews*, **72**(1), 21–38.

Maaløe, S. & Scheie, Å., 1982. The permeability controlled accumulation of primary magma. *Contributions to Mineralogy and Petrology*, **81**, 350–357.

Macdonald, G. A., 1968. Composition and origin of hawaiian lavas. *Geological Society of America Memoirs*, **116**, 477–522.

Martin, H., 1986. Effect of steeper Archean geothermal gradient on geochemistry of subduction-zone magmas. *Geology*, **14**(9), 753–756.

Martin, H. & Moyen, J.-F., 2002. Secular changes in tonalite-trondhjemite-granodiorite composition as markers of the progressive cooling of Earth. *Geology*, **30**(4), 319–322.

Mayne, M. J., Moyen, J. F., Stevens, G. & Kaislaniemi, L., 2016. Rcrust: a tool for calculating path-dependent open system processes and application to melt loss. *Journal of Metamorphic Geology*, DOI:10.1111/jmg.12199.

Middlemost, E. A., 1994. Naming materials in the magma/igneous rock system. *Earth-Science Reviews*, **37**(3), 215–224.

Milord, I., Sawyer, E. W. & Brown, M., 2001. Formation of diatexite migmatite and granite magma during anatexis of semi-pelitic metasedimentary rocks: an example from St. Malo, France. *Journal of Petrology*, **42**, 487–505.

Mottl, M. J. & Holland, H. D., 1978. Chemical exchange during hydrothermal alteration of basalt by seawateri. experimental results for major and minor components of seawater. *Geochimica et Cosmochimica Acta*, **42**(8), 1103–1115.

Moyen, J.-F. & Martin, H., 2012. Forty years of TTG research. *Lithos*, **148**, 312–336.

Moyen, J.-F. & Stevens, G., 2006. Experimental constraints on TTG petrogenesis: implications for Archean geodynamics. *Archean geodynamics and environments*, pp. 149–175.

Nockolds, S. & Le Bas, M., 1977. Average calc-alkali basalt. *Geological Magazine*, **114**(04), 311–312.

Palin, R. M., White, R. W., Green, E. C. R., Diener, J. F. A., Powell, R. & Holland, T. J. B., 2016. High-grade metamorphism and partial melting of basic and intermediate rocks. *Journal of Metamorphic Geology*, DOI: 10.1111/jmg.12212.

Park, R. G., 1966. Nature and origin of lewisian basic rocks of gairloch, ross-shire. *Scottish Journal of Geology*, **2**(2), 179–199.

Patino-Douce, A. & Johnston, A. D., 1991. Phase equilibria and melt productivity in the pelitic system: implications for the origin of peraluminous granitoids and aluminous granulites. *Contributions to Mineralogy and Petrology*, **107**(2), 202–218.

Peacock, S. M., Rushmer, T. & Thompson, A. B., 1994. Partial melting of subducting oceanic crust. *Earth and planetary science letters*, **121**(1), 227–244.

Powell, R. & Holland, T. J. B., 1988. An internally consistent thermodynamic dataset with uncertainties and correlations: 3. Application, methods, worked examples and a computer program. *Journal of Metamorphic Geology*, **6**, 173–204.

Rapp, R. P., Shimizu, N. & Norman, M. D., 2003. Growth of early continental crust by partial melting of eclogite. *Nature*, **425**(6958), 605–609.

Rapp, R. P., Watson, E. B. & Miller, C. F., 1991. Partial melting of amphibolite/eclogite and the origin of Archean trondhjemites and tonalites. *Precambrian Research*, **51**(1), 1–25.

Rebay, G., Powell, R. & Diener, J. F. A., 2010. Calculated phase equilibria for a MORB composition in a P–T range, 450–650°C and 18–28 kbar: the stability of eclogite. *Journal of Metamorphic Geology*, **28**, 635–645.

Robertson, J. & Wyllie, P., 1971. Rock-water systems, with special reference to the water-deficient region. *American Journal of Science*, **271**(3), 252–277.

Rosenberg, C. L. & Handy, M. R., 2005. Experimental deformation of partially melted granite revisited: implications for the continental crust. *Journal of Metamorphic Geology*, **23**, 19–28.

Rudnick, R. & Taylor, S., 1987. The composition and petrogenesis of the lower crust: a xenolith study. *Journal of Geophysical Research: Solid Earth*, **92**(B13), 13981–14005.

Rudnick, R. L. & Fountain, D. M., 1995. Nature and composition of the continental crust: a lower crustal perspective. *Reviews of geophysics*, **33**(3), 267–309.

Rudnick, R. L.et al., 1995. Making continental crust. *Nature*, **378**(6557), 571–577.

Rushmer, T., 1991. Partial melting of 2 amphibolite - contrasting experimental results under fluid-absent conditions. *Contributions to Mineralogy and Petrology*, **107**, 41–59.

Sawyer, E. W., 1987. The role of partial melting and fractional crystallisation in determining discordand migmatite leucosome compositions. *Journal of Petrology*, **32**, 701–738.

Sawyer, E. W., 1994. Melt segregation in the continental crust. *Geology*, **22**, 1019–1022.

Sawyer, E. W., 2001. Melt segregation in the continental crust: Distribution and movement of melt in anatectic rocks. *Journal of Metamorphic Geology*, **19**, 291–309.

Sawyer, E. W., 2008. *Atlas of Migmatites, The Canadian Mineralogist Special Publication 9*, NRC Research Press, Ottawa, Ontario.

Sawyer, E. W., Cesare, B. & Brown, M., 2011. When the continental crust melts. *Elements*, **7**, 229–234.

Seyfried, W. E. & Mottl, M. J., 1982. Hydrothermal alteration of basalt by seawater under seawater-dominated conditions. *Geochimica et Cosmochimica Acta*, **46**(6), 985–1002.

Stern, C. R., Huang, W. L. & Wyllie, P. J., 1975. Basalt-andesite-rhyolite-H_2O: Crystallization intervals with excess H_2O and H_2O-undersaturated liquidus surfaces to 35 kolbras, with implications for magma genesis. *Earth and Planetary Science Letters*, **28**(2), 189–196.

Sun, S. S. & McDonough, W. F., 1989. Chemical and isotopic systematics of oceanic basalts: implications for mantle compositions and processes, *Magmatism in the Ocean Basins*, Vol. 42, pp. 313–345. The Geological Society, London, Special Publication.

Thompson, A. B., 1982. Dehydration melting of pelitic rocks and the generation of H_2O-undersaturated granitic liquids. *American Journal of Science*, **282**(10), 1567–1595.

Thompson, A. B. & Connolly, J. A., 1995. Melting of the continental crust: some thermal and petrological constraints on anatexis in continental collision zones and other tectonic settings. *Journal of Geophysical Research: Solid Earth*, **100**(B8), 15565–15579.

Thompson, A. B. & England, P. C., 1984. Pressure-Temperature-time paths of regional metamorphism II. Their inference and interpretation using mineral assemblages in metamorphic rocks. *Journal of Petrology*, **25**(4), 929–955.

Turner, S. & Hawkesworth, C., 1995. The nature of the sub-continental mantle: constraints from the major-element composition of continental flood basalts. *Chemical Geology*, **120**(3), 295–314.

Vielzeuf, D. & Holloway, J. R., 1988. Experimental determination of the fluid-absent melting relations in the pelitic system - consequences for crustal differentiation. *Contributions to Mineralogy and Petrology*, **98**(3), 257–276.

Vielzeuf, D. & Schmidt, M., 2001. Melting relations in hydrous systems revisited: application to metapelites, metagreywackes and metabasalts. *Contributions to Mineralogy and Petrology*, **141**(3), 251–267.

Vielzeuf, D., Clemens, J., Pin, C. & Moinet, E., 1990. Granites, granulites, and crustal differentiation, *Granulites and crustal evolution*, pp. 59–85. Springer.

Vigneresse, J. L., Barbey, P. & Cuney, M., 1996. Rheological transitions during partial melting and crystallization with application to felsic magma segregation and transfer. *Journal of Petrology*, **37**, 1579–1600.

Weinberg, R. F., 1999. Mesoscale pervasive felsic magma migration: alternatives to dyking. *Lithos*, **46**, 393 – 410.

Wells, P., 1980. Thermal models for the magmatic accretion and subsequent metamorphism of continental crust. *Earth and Planetary Science Letters*, **46**(2), 253–265.

White, R. & McKenzie, D., 1989. Magmatism at rift zones: the generation of volcanic continental margins and flood basalts. *Journal of Geophysical Research: Solid Earth*, **94**(B6), 7685–7729.

White, R. W. & Powell, R., 2002. Melt loss and the preservation of granulite facies mineral assemblages. *Journal of Metamorphic Geology*, **20**, 621–632.

White, R. W. & Powell, R., 2010. Retrograde melt–residue interaction and the formation of near-anhydrous leucosomes in migmatites. *Journal of Metamorphic Geology*, **28**, 579–597.

White, R. W., Powell, R. & Halpin, J. A., 2004. Spatially-focussed melt formation in aluminous metapelites from Broken Hill, Australia. *Journal of Metamorphic Geology*, **22**, 825–845.

White, R. W., Powell, R. & Holland, T. J. B., 2001. Calculation of partial melting equilibria in the system Na_2O–CaO–K_2O–FeO–MgO–Al_2O_3–SiO_2–H_2O (NCKFMASH). *Journal of Metamorphic Geology*, **19**, 139–153.

White, R. W., Powell, R. & Holland, T. J. B., 2007. Progress relating to calculation of partial melting equilibria for metapelites. *Journal of Metamorphic Geology*, **25**, 511–527.

White, R. W., Powell, R. & Johnson, T. E., 2014. The effect of Mn on mineral stability in metapelites revisited: new a–x relations for manganese-bearing minerals. *Journal of Metamorphic Geology*, **32**, 809–828.

Winkler, H. G., 1979. Anatexis, formation of migmatites, and origin of granitic magmas, *Petrogenesis of metamorphic rocks*, pp. 283–339. Springer.

Wolf, M. B. & Wyllie, P. J., 1994. Dehydration-melting of amphibolite at 10 kbar: the effects of temperature and time. *Contributions to Mineralogy and Petrology*, **115**(4), 369–383.

Wyllie, P. J. & Wolf, M. B., 1993. Amphibolite dehydration-melting: sorting out the solidus. *Geological Society, London, Special Publications*, **76**(1), 405–416.

Yakymchuk, C. & Brown, M., 2014. Consequences of open-system melting in tectonics. *Journal of the Geological Society*, **171**, 21–40.

Zandt, G., Ammon, C. J.et al., 1995. Continental crust composition constrained by measurements of crustal Poisson's ratio. *Nature*, **374**(6518), 152–154.

Zen, E.et al., 1988. Phase relations of peraluminous granitic rocks and their petrogenetic implications. *Annual Review of Earth and Planetary Sciences*, **16**, 21.

Zhang, C., Holtz, F., Koepke, J., Wolff, P. E., Ma, C. & Bédard, J. H., 2013. Constraints from experimental melting of amphibolite on the depth of formation of garnet-rich restites, and implications for models of Early Archean crustal growth. *Precambrian Research*, **231**, 206–217.